USE OF ZnS AS A SELF-FOCUSING ELEMENT IN A SELF-STARTING KERR LENS MODELOCKED Ti:SAPPHIRE LASER

BY

GARY WHITON PEARSON

Bachelor of Arts
Pennsylvania State University
State College, Pennsylvania
1976

Bachelor of Science
Oklahoma State University
Stillwater, Oklahoma
1984

Masters of Science
Rutgers, the State University
New Brunswick, New Jersey
1987

Submitted to the Faculty of the
Graduate College of the
Oklahoma State University
in partial fulfillment of
the Degree of
DOCTOR OF PHILOSOPHY
May, 1993

OKLAHOMA STATE UNIVERSITY

USE OF ZnS AS A SELF-FOCUSING ELEMENT IN

A SELF-STARTING KERR LENS MODELOCKED

Ti:SAPPHIRE LASER

Thesis Approved:

Thesis Advisor

Dean of the Graduate College

ACKNOWLEDGMENTS

I wish to express my gratitude to the individuals who assisted me in this project and during my coursework at Oklahoma State University. In particular, I wish to thank my major advisor, Dr. Jerzy S. Krasinski, for his guidance, inspiration, and invaluable aid. Also, I would like to thank Dr. Czeslaw Radzewicz, for his help in the experimental details of the project. Additionally, I wish to thank Dr. Hans Bilger for his help in getting me started in the world of lasers, and Dr. Keith Teague for his helping me to understand efficient methods to tackle complex computer algorithms. Since the project involved the marriage of numerical, theoretical, and experimental methods, the skills given to me by each of these individuals has proven to be absolutely invaluable for the success of the research. Equally important was their friendship and encouragement. The fact that these individuals devoted as much of their own time as they did to my education and research is something I still find rather incredible. I can neither thank nor praise them enough.

Invaluable friendship and the encouragement to continue along the path was also given by Dr. Jim West, Dr. Tom

Gedra, Dr. Yehuda Band, and Dr. Ray Zanoni. Again, I feel that studying at OSU has provided me with a unique experience that simply could not have been gained at any other institution. This is because of the people, like those mentioned above, that make up the outstanding faculty here.

Special thanks is certainly due the taxpayers of this State, as well as the leaders that made the initial decision to invest in the OSU Laser Center. The fact that the people of this State decided to take such a chance on the facilities and in people like me means that I will owe them something for the rest of my years. Additionally, I wish to thank the people of WilTel, Inc., for their faith in our ability to assist them through what must have seemed a somewhat bizarre, from their perspective, research direction. Nonetheless, they supported us all the way.

Of course, it should go without saying the thanks and gratitude that I have for my wife, Carol, and my son, Bob, for their support and their encouragement throughout the journey. It isn't every wife that would not only allow, but absolutely encourage, her middle-aged spouse to quit a full-time, well paying job to pursue his educational goals. But, like I have already said, the people I have had the luck to meet and be with just aren't typical people, so again, I feel blessed.

I sincerely hope the reader finds the results in this report both interesting and useful.

TABLE OF CONTENTS

LIST OF TABLES

LIST OF FIGURES

CHAPTER I

INTRODUCTION

A recent technology, Kerr Lens Modelocking (KLM) in a Ti:sapphire laser, first demonstrated by Spence, et al. [1], has led to the development of solid-state lasers that are capable of producing pulses as short as 17-fs [2]. KLM lasers (also known as self-modelocked lasers, since initially they seemed to modelock 'by themselves' [1]) have certain advantages over those femtosecond lasers that use other passive modelocking technologies in terms of ease of operation and lower maintenance. For example, there need not be saturable dye-jets in a KLM laser, as is the case in colliding pulse femtosecond lasers [3]. Added to the advantage of operational simplicity is that of wide tunability. With a bandwidth spanning from 750nm to 1050nm [4], a Ti:sapphire KLM laser is a fairly versatile tool for the production of ultra-short pulses. With the application of Optical Parametric Oscillator (OPO) techniques, KLM Ti:sapphire lasers have been built from which it is possible to produce sub-100 fs pulses across the wavelength range of from 0.9 to 4.5 μm [5][6]. KLM Ti:sapphire lasers have also been used to produce femtosecond pulses amplified up to TW powers [7][8]. Since the announcement of the success of

Spence, *et al.* in 1990 until today, no less than four companies have begun marketing some version of the KLM Ti:sapphire femtosecond laser [9]. Thus it would seem that KLM Ti:sapphire lasers, currently widely available commercially, would become the laser of choice for those requiring relatively high power, ultra-fast and highly tunable pulses.

However, there is still room for improvement in these lasers. First is that of an expensive, relatively high power pump laser required for femtosecond operation. Though the Ti:sapphire KLM laser is itself a solid-state laser, it is most often pumped with an argon-ion laser. Because many Ti:sapphire KLM lasers require between 6 and 10 W of pumping power to allow femtosecond operation, these argon-ion lasers tend to be rather large and expensive. This adds to the overall expense of the femtosecond pulse generation system.

A second concern is that of self-starting in KLM lasers. A self-starting KLM laser is one that has the ability to modelock without additional modelocking methods being employed. Typically, a Ti:sapphire KLM laser will not self-start. Tamura, et al.,[10] announced recently a unidirectional KLM Ti:sapphire ring-laser that will self-start. This is done by reducing back reflections, which are thought to compete in a linear cavity in the modelocking process. In linear cavity KLM Ti:sapphire lasers, there are no known reports of a method that results in consistent self-starting, except for that described in this report.

There have been numerous other solutions to the self-starting issue in linear cavity KLM Ti:sapphire lasers. These including the use of an intracavity saturable dye jet [11], coupling with a cavity that contains a slowly modulated high reflection mirror [12] [13], the use of an intracavity acousto-optic modulator [14], coupling with a cavity that contains a nonlinear multi-quantum well reflector [15], coupling to a cavity that contains a semiconductor saturable absorber [16], the precise alignment of the Ti:sapphire cavity length (to within 10 microns) to the length of the pump argon ion laser [17], and the use of a shaker [18]. However, each of these methods requires an added level of complexity either in additional maintenance, as is the case when dye jets are used, an added expense, as when a custom made semiconductor is used, or more difficult alignment is required, as when a coupled cavity is employed.

Related to the issue of self-starting is that of the stability of modelocked operation of these lasers. For, without some kind of additional modelocking mechanism or an active 're-modelocking' mechanism, the typical KLM laser will remain modelocked only for relatively short periods of time, on the order of a half-hour or so [1].

Earlier work by Chen and Wang [11] showed that these three problems found in most KLM Ti:sapphire lasers: high pump power requirements, lack of self-starting, and poor

long term stability, were related to the small nonlinear response of the modelocking medium, Ti:sapphire. The nonlinear index of refraction, n_2, is equal to 3.0 x 10^{-20} m^2/W [19] at a wavelength of 800 nm, the location of peak gain for Ti:sapphire [4]. (Note that Appendix F gives the details of how the values for n^2 were arrived at in this study.) This compares to a material like ZnS, which has a nonlinear index of refraction roughly 30 times higher than that of Ti:sapphire. Briefly, KLM lasers use a combination of self-focusing in a nonlinear medium and an intracavity aperture to act as a modelocking mechanism. In the KLM modelocked laser, an intensity dependent lens and an intracavity aperture are aligned such that for high power pulses, self-focusing results in a decrease in loss at the aperture [20]. Because the self-focusing effect is proportional to the nonlinear index of refraction, n_2, a weakly nonlinear material like Ti:sapphire requires a relatively high intracavity intensity to self-modelock.

Although the n_2 of Ti:sapphire can not be increased, the overall n_2 of the cavity can be increased. This can be accomplished by the addition of an element with higher n_2 into the cavity. Note that the addition of a highly nonlinear element was first used by Malcolm and Ferguson [21] to self-modelock a picosecond Nd:YLF laser using a piece of intracavity SF57 glass as a self-focusing lens. The addition of a highly nonlinear element to make the cavity more

nonlinear can be likened to making the overall dispersion of a given laser cavity more negative by the addition of an intracavity negative dispersion prism pair [22].

The main thrust of this report will be an examination of the use of an additional highly nonlinear intracavity self-focusing element in a Ti:sapphire self-modelocked laser as a technique to assist in the modelocking of a linear cavity KLM Ti:sapphire laser. By the addition of an intracavity highly nonlinear element that acts as a self-focusing lens, this report will show that it is possible to:

1) lower pump power requirements for modelocked operation,

2) make a linear cavity Ti:sapphire KLM laser self-starting, and

3) improve the long term stability of the laser.

The first part of this report is a summary of the numerical simulations accomplished that showed for the first time that self-focusing modelocking is quite unlike a saturable absorber [23], which it has been very often modelled as by other researchers [11][17]. Note that the numerical results summarized in this report have since been replicated by Heatley, et al. [24].

The second part of this report is a summary of the experimental work done at the OSU Laser Research Center to test various types of nonlinear materials for use as an

additional self-focusing lens in a KLM Ti:sapphire laser [25]. The best results were obtained using a 3.75 mm thick piece of monocrystalline ZnS, which has a calculated nonlinear index of refraction of $n_2 = 90 \times 10^{-20}$ m^2/W. The use of ZnS allowed for the construction of the first linear cavity Ti:sapphire KLM laser that consistently self-starts and remains self-modelocked for periods up to at least 12 hours without restarting. Additionally, the minimum pump power requirement to sustain self-modelocking was reduced by more than a factor of 2 when ZnS was placed in the cavity. It should be noted that the results obtained here at OSU using monocrystalline ZnS in a linear cavity KLM Ti:sapphire laser have since been partially replicated elsewhere [26]. Additionally, it is important to point out that while the work that has gone on here at OSU is directed at the use of an additional self-focusing lens in a Ti:sapphire laser, the method may in future also be applied to the passive modelocking of all solid-state (diode pumped) femtosecond KLM systems, such as Cr:LiSAF lasers [27] [28].

CHAPTER II

MODELOCKING IN KERR LENS MODELOCKED LASERS

Accurate modelling of the propagation of a beam through a nonlinear medium presents a reasonable challenge. This is because, except for very specific waveforms (i.e., solitons [29]) general analytical solutions for this problem do not exist. Therefore, in order to model an arbitrary waveform propagating through a nonlinear medium, one is forced to employ numerical methods.

Mode-locking is the process of forcing the relative phases of the many longitudinal modes in a continuous wave (cw) laser to zero [3]. The result is that the output of a mode-locked laser becomes a train of short pulses with the period between the pulses equal to the cavity round trip time. Since a very narrow pulse requires a very wide spectrum [30], the narrowness of the modelocked pulse is limited by the bandwidth spanned by the longitudinal modes. Thus, a material like Ti:sapphire, with a gain bandwidth of over 300 nm, has the capability of supporting pulses in the femtosecond range. As an estimate to the limit the gain bandwidth of Ti:sapphire imposes on pulse duration in a KLM laser, we may use the relation for a transform-limited Gaussian zero-chirp pulse [4]

$$\tau_p = \frac{0.441}{\Delta\nu} \qquad \text{(Eq. 1)}$$

where τ_p is the *1/e* pulse width and $\Delta\nu$ is the gain bandwidth of Ti:sapphire equal to [4]

$$\Delta\nu = \frac{c}{750\ \text{nm}} - \frac{c}{1050\ \text{nm}}$$

$$= 128\ \text{THz}$$

This means that the shortest pulses one can achieve directly from a modelocked Ti:sapphire laser are roughly τ_p = 3.4 fs. Note that the shortest pulses from a KLM Ti:sapphire laser reported thus far are 14.5 fs [31]. There are many processes in the laser that might act to broaden a femtosecond pulse, including:

1) first and second order group velocity dispersion (GVD) [32],

2) Self-Phase Modulation (SPM) [17],

3) the bandwidth limit of the mirrors used in the cavity,

4) the gain limited bandwitdh of the laser, and,

5) self-focusing in the nonlinear medium [22].

The first two limitations listed above, GVD and SPM, can occur when the intracavity pulse propagates through the prisms, the gain medium, and even the output coupler in a laser [31]. A combination of GVD and SPM such that pulse spreading does not occur even for femtosecond pulses has been called a soliton effect [33]. Some researchers

describe the multi-pulsing phenomena seen in KLM Ti:sapphire lasers as evidence for higher order solitons in an over-pumped lasers [34]. Krausz, et al., have shown that the pulse width varies greatly from one side of the laser to the other, and choose to describe the lasers as soliton-like, or 'solitary' lasers [17]. For mirrors with multi-layered dielectric mirrors, the many layers can act something like a Fabrot-Perot, thus broadening the pulse with each reflection. The solution often sought is to employ only single-layered mirrors. The effect of gain bandwidth has already been discussed above. The ability of self-focusing to limit the modelocking process was first shown by Pearson, Radzewicz, and Krasinski [23], and will be discussed further in this report.

All passive modelocking methods employ some kind of intensity dependent gain in the laser cavity to produce short pulses from the initially almost random intracavity beam intensity envelope that one would expect to see in a cw laser running on many longitudinal modes simultaneously. The view that self-focusing is the major modelocking mechanism in a KLM laser cavity was originally developed by Piche' [20]. According to this view, KLM lasers use self-focusing as a modelocking mechanism in the following manner. For high optical field intensities, the index of refraction, n, of a nonlinear medium is given as

$$n = n_0 + n_2 I \qquad \text{(Eq. 2)}$$

where n_0 is the linear index of refraction, n_2 is the nonlinear index coefficient, and I is the intensity of the optical field [35]. For a beam with the maximum intensity on axis, and a beam distribution in which the intensity decreases monotonically with the distance from the beam axis (e.g.; Gaussian or hyperbolic secant beam profile) the higher intensity found on axis results in a greater phase change of the beam as it travels through the nonlinear medium. In this manner, a flat nonlinear element acts as a power dependent lens.

According to Piche', KLM lasers exploit the power dependence of the self-focusing effect to discriminate in favour of high instantaneous power. An aperture is placed in the cavity in such a way that initially it blocks a few percent of the intracavity beam power. Fig. 1, in Appendix H, shows a simplified KLM laser cavity in which two beam profiles are shown, one for low power and one for high power. The high power beam profile experiences less loss at the aperture due to self-focusing. Note that, on a time scale of femtoseconds, even a cw beam will display a rapidly varying intensity profile for a laser operating on many longitudinal modes, since we have beating between many, many modes (on the order of 10^4-10^5). Therefore, higher power portions of the rapidly varying pulse envelope will experience more self-focusing compared to the lower power temporal portions of the beam. For a properly placed aperture, this slight

focusing results in a smaller beam diameter at the aperture, and thus translates into lower losses for these high power portions of the rapidly varying cw envelope. Piche' discusses two kinds of apertures in his work: hard and soft. A hard aperture could be an edge of a prism or an actual slit placed in the cavity, while a soft aperture is seen as the interaction of pump and cavity beam profiles in the gain medium. For either hard or soft apertures, self-focusing results in larger gain for the high intensity portions of the beam.

In the absence of any competing effects, the ability of even a seemingly small discrimination between intensities to force a laser to modelock can be seen in the following first-order modelocking computer simulation example. Appendix A shows more of the details of this numerical simulation. Note that the loss vs. power relation for a KLM laser is not linear, a point that will be developed further in the text. However, as a first-order approximation, one may take the differential loss in an initially free-running laser to be:

$$loss = loss_0 + \gamma P \qquad \text{(Eq. 3)}$$

where $loss_0$ is aperture loss per cavity round-trip at zero power, which might be typically be 4% for a high gain laser, γ is the slope of the loss vs. power curve, and P is instantaneous intracavity power. In this case, the slope found in

the simulations presented in this report of very highly nonlinear self-focusing elements, where initially $\gamma = 10^{-5}$ W^{-1}, was used.

Assuming that pulse envelope of the combination of some 10^4 to 10^5 longitudinal modes present within the cavity of a free-running Ti:sapphire laser will closely resemble noise, the simulation was started with a random distribution of the intracavity power with an average power of 15 W (shown in Fig. 2). For a 10% output coupler, this would translate into a 1.5 W laser, which is about typical for KLM Ti:sapphire lasers. After 2000 round trips through the cavity using the linear loss rule above and normalizing power at each step, we see that what before resembled noise has progressed into the beginnings of a modelocked laser as a number of distinct peaks have developed (shown in Fig. 3). Lower intensity portions of the time domain intracavity beam are eventually eliminated by their higher loss, while higher intensity portions of the beam tend to grow, until finally, only one pulse remains in the intracavity beam. After 5000 round trips (shown in Fig. 4) we see that only one narrow peak remains, and the numerical laser is now fully modelocked.

Of course, even if the initial phase of modelocking is described well by a linear relation between loss vs. intracavity power, one would expect that the differential gain for high power pulses would eventually saturate. This is

the case of the classic saturable absorber, as will be discussed more in a later section. Otherwise, the loss vs. power curve would eventually cross the zero loss axis (*i*.e., the nonlinear element would produce gain in the cavity.)

CHAPTER III

GAUSSIAN THIN LENS MODEL OF SELF-MODELOCKING

Though the one of the goals is to develop a more complete model of Kerr lens modelocking, it will instructional to begin with a much simpler method. The simplest model would be to approximate the effects of a self-focusing lens with a Gaussian thin lens model. In this section, we will look at the effect of placing a Gaussian thin lens with a power dependent focus in a cavity of a laser with an intracavity aperture. Fig. 5 shows a schematic of the unfolded non-symmetric cavity that was used in the thin-lens modelling of a self-focusing element in a KLM laser cavity.

The cavity used for the thin-lens self-focusing simulation contained four mirrors, with an initial beam waist between mirrors M_2 and M_3 of approximately 30 μm. Mirrors M_1 and M_4 were flat, while mirrors M_2 and M_3 had a radius of 10 cm. In this cavity, an aperture was placed directly in front of mirror M_4 to act as a modelocking discriminator. The distance between M_1 and M_2 was 50 cm, and the distance from M_3 to M_4 was 75 cm. The optical distance between M_2 and M_3 was about 10.5 cm. As was previously found by Chen and Wang [11], placing the nonlinear lens slightly away from the waist resulted in the desired decrease in aperture

loss for higher intracavity powers for this particular cavity. Thus, the power dependent Gaussian thin lens, L_p, used to give a first-order approximation of the effects of self-focusing in this cavity was placed slightly (1 mm) away from the location of the beam waist between M_2 and M_3.

The Gaussian approximation is based on the propagation of the complex beam parameter, q, in a self-consistant manner such that [36]

$$q = \frac{qA + B}{qD + C} \qquad \text{(Eq. 4)}$$

where A, B, C, and D are the elements of the Gaussian ABCD matrix

The ABCD matrix for propagation through a homogeneous medium is simply [36]

$$M_{free\text{-}space} = \begin{bmatrix} 1 & d \\ 0 & 1 \end{bmatrix} \qquad \text{(Eq. 5)}$$

where d is the optical length of the material.

The distance matrices for the particular cavity studied become

$$D_1 = \begin{bmatrix} 1 & 0.5 \\ 0 & 1 \end{bmatrix}$$

$$D_2 = \begin{bmatrix} 1 & 0.0515 \\ 0 & 1 \end{bmatrix}$$

$$D_3 = \begin{bmatrix} 1 & 0.0535 \\ 0 & 1 \end{bmatrix}$$

$$D_4 = \begin{bmatrix} 1 & 0.75 \\ 0 & 1 \end{bmatrix}$$

The ABCD matrix of a thin lens/mirror is given as

$$M_{lens/mirror} = \begin{bmatrix} 1 & 0 \\ -1/f & 1 \end{bmatrix} \qquad \text{(Eq. 6)}$$

where f is the focal length of the lens or mirror. Using MKS units throughout, the matrices for mirrors M_1, M_2, M_3 and M_4 are given as [36]

$$M_1 = \begin{bmatrix} 1 & 0 \\ 0 & 1 \end{bmatrix}$$

$$M_2 = \begin{bmatrix} 1 & 0 \\ -2/R & 1 \end{bmatrix}$$

$$= \begin{bmatrix} 1 & 0 \\ -20 & 1 \end{bmatrix}$$

$$M_3 = \begin{bmatrix} 1 & 0 \\ -20 & 1 \end{bmatrix}$$

$$M_4 = \begin{bmatrix} 1 & 0 \\ 0 & 1 \end{bmatrix}$$

and that of the self-focusing (power dependent focus) thin lens is given as

$$L_P = \begin{bmatrix} 1 & 0 \\ -1/f_{LP} & 1 \end{bmatrix} \qquad \text{(Eq. 7)}$$

To examine the change in the beam radius at the aperture in from of mirror M_4, the round trip cavity matrix, M_{cavity}, of the cavity studied is calculated as

$$M_{cavity} = D_4 M_3 D_3 L_P D_2 \qquad \text{(Eq. 8)}$$
$$\times M_2 D_1 M_1 D_1 M_2 D_2 L_P D_3 M_3 D_4 M_4$$

Note that because the matrices for M_1 and M_4 are the indentity matrix, simplification can be achieved by leaving them out of the calculation, reducing the cavity round trip matrix to

$$M_{cavity} = D_4 M_3 D_3 L_P D_2 M_2 \times D_1 D_1 M_2 D_2 L_P D_3 M_3 D_4 \quad \text{(Eq. 9)}$$

The complex beam parameter q is obtained from the resulting ABDC matrix as [36]

$$\frac{1}{q} = -\frac{(A-D)}{2B} - \frac{i}{B}\sqrt{1-[(A+D)/2]^2} \quad \text{(Eq. 10)}$$

where the complex beam parameter is given as [36]

$$\frac{1}{q} = \frac{1}{R} - i\frac{\lambda}{\pi w(z)^2} \quad \text{(Eq. 11)}$$

Beam radius w(z) is then extracted from the beam parameter q

$$w(z) = \sqrt{\frac{-\mathrm{Im}(q)\pi}{\lambda}} \quad \text{(Eq. 12)}$$

where Im(q) is the imaginary portion of q.

Using a computer program to perform the matrix multiplication and the above algebra, it is a simple matter to examine the beam radius, w(z), at the aperture as a function of the focal length of the thin self-focusing lens L_P. Table 1 shows a comparison of these two parameters of interest. The focal length of infinity is equivalent to low power operation of the laser. Shorter and shorter focal lengths correspond to higher and higher instantaneous intracavity power in the laser.

Table I

GAUSSIAN THIN-LENS APPROXIMATION

focal length (cm) of L_p	beam radius at M_4 (mm)
∞	0.680
100	0.668
50	0.657
25	0.637
15	0.615
5	0.542
1	0.405
0.5	0.354
0.2	0.323
0.15	0.361
0.14	0.397
0.13	0.523
0.128	0.626
0.127	0.767
0.1265	0.995
0.1260	unstable cavity

From Table 1, one can see that there is an initial decrease of the beam radius at the aperture with a decrease in focal length of self-focusing lens L_p, which corresponds to an increase in intracavity power. However, as the focal length of the self-focusing lens L_p becomes very small, a condition that would correspond to very high pulse peak power, the beam radius at M_4 starts to grow rapidly. Eventually, for a focal length of about 0.126 cm in this example, the cavity becomes unstable.

Keeping in mind the limitations of this simple model, such as the thin lens approximation as well as beam diffraction at the aperture being ignored, one could interpret the results as follows. Initially, for a properly placed aperture, higher power portions of the intracavity temporal waveform experience lower loss, and therefore see a larger gain in a cavity with amplification (e.g., a laser). This is consistent with Piche's model of self-focusing modelocking.

However, it is interesting to note that even in this simplest model of a KLM laser, the relationship between increase in intracavity instantaneous power (modelled here as the shortening of the focal length of L_p) and intracavity loss (here modelled as beam radius at the aperture) is non-monotonic. As such, a minimum loss power exists for a given cavity configuration. Further increases in instantaneous intracavity power result in higher losses. This suggests

that for a given laser configuration and average intracavity power, self-focusing will act eventually to limit the pulse shortening process. Also, very high focusing power results in an unstable resonator cavity. This is perhaps of less interest, since one generally assumes that a laser tends to run where losses are the least. This might mean that once the minimum loss power is reached, pulse shortening ceases. Thus the higher, unstable pulse power regimes are never reached.

These two characteristics of the self-modelocking process in a KLM laser make self-focusing modelocking a fundamentally different kind of passive modelocking device, quite different from a classic saturable absorber. One will recall that a classical saturable absorber will 'bleach' [4], such that higher and higher pulse powers will result in essentially the same loss once bleaching has occurred. Put most simply, a self-focusing lens does not bleach. However, due to the small amount of faith one can put in this overly simplified model, this idea was pursed more fully using more accurate models of the KLM laser.

CHAPTER IV

PARABOLIC GRIN LENS RAY MATRIX APPROXIMATION OF SELF-MODELOCKING

A higher order model that takes into account the thickness of the nonlinear medium that was used to model beam propagation through a nonlinear medium was to approximate the medium as a power dependent parabolic index of refraction profile GRIN lens [19][20][37][38]. In Appendix B it is shown how the parabolic profile ABCD matrix is obtained for a self-focusing lens as

$$L_P = \begin{bmatrix} \cos\left(\frac{d}{\beta}\right) & \beta\sin\left(\frac{d}{\beta}\right) \\ -\frac{1}{\beta}\sin\left(\frac{d}{\beta}\right) & \cos\left(\frac{d}{\beta}\right) \end{bmatrix} \qquad \text{(Eq. 13)}$$

where d is the optical length of the material and β depends on the beam radius, w(z), intensity, I, and the linear and nonlinear index of refraction, n_0 and n_2 respectively, according to

$$\beta = \frac{w(z)}{2}\sqrt{\frac{n_0 + n_2 I_0}{n_2 I_0}} \qquad \text{(Eq. 14)}$$

For an estimate of the focusing power of a typical self-focusing lens in a KLM Ti:sapphire laser we can look at a practical example. Lemoff and Barty report a Ti:sapphire laser with an output peak pulse power of 0.5 MW using a 10%

transmission output coupler [39]. This means that the intracavity pulse peak power in their laser was about 5 MW. Using a more moderate intracavity pulse peak power of 1 MW, a linear index of refraction of Ti:sapphire of $n_0 = 1.76$, a nonlinear index of refraction of $n_2 = 3.0 \times 10^{-20}$ m^2/W, and a beam radius at the focus of 20 μm, we see that in a typical KLM Ti:sapphire laser

$$\beta = \frac{20\times10^{-6}}{2}\sqrt{\frac{1.76+(3.0\times10^{-20}\mathrm{m^2/W})(3.18\times10^{15}\mathrm{W/m^2})}{(3.0\times10^{-20}\mathrm{m^2/W})(3.18\times10^{15}\mathrm{W/m^2})}}$$

$$= 1.36\mathrm{mm}$$

For an extremely short piece of Ti:sapphire, for example a 0.1 mm piece, the ABCD matrix (using MKS units) becomes

$$L_{0.1\ mm} = \begin{bmatrix} \cos(0.0736) & 0.0014\sin(0.0736) \\ -735\sin(0.0736) & \cos(0.0736) \end{bmatrix}$$

$$= \begin{bmatrix} 0.997 & 0.1\times10^{-3} \\ -54 & 0.997 \end{bmatrix}$$

If we compare this matrix to that of a simple thin lens, given as

$$M_L = \begin{bmatrix} 1 & 0 \\ -\frac{1}{f} & 1 \end{bmatrix} \qquad \text{(Eq. 15)}$$

we see that the focal length of this self-focusing lens example when modelled as a simple thin-lens is about 1.85 cm. In a laser cavity that is often more than a meter long, this may represent considerable beam re-shaping, depending on the placement of the nonlinear lens.

Note that the actual rod length in a Ti:sapphire laser is typically between 4 mm [31] and 20 mm [1]. Additionally, the beam radius, w(z), and the intensity of the beam on axis, I_0, vary considerably from one end of the rod to the other. One method used to treat this variation in w(z) and I_0 is to divide the rod up into a number of parabolic lens [19]. Such a process is iterative in nature, since the effect of the lens is to change I_0 for the following parabolic lens segment, which of course changes the focusing properties of that lens segment.

Another method used that has been used is to simply use the beam confocal parameter, z_0, given as [36]

$$z_0 = \frac{\pi w_0^2}{\lambda} \qquad \text{(Eq. 16)}$$

as an effective nonlinear length of the laser rod [12] along with an average intensity. The philosophy here is that only the area near the focus of the beam contributes significantly to the nonlinear phase shift, since this is where the beam intensity is highest.

It should be noted that a fit of an exponential index profile to that of a parabolic profile leads to a poor estimate of the self-focusing effect in the wings of the beam. Fig. 6 shows a comparison of the parabolic fit to a normalized Gaussian distribution with both I_0 and w_0 equal to unity. As can be seen from the figure, the parabolic fit works well on axis, where the intensity is the greatest for

a TEM_{00} Gaussian beam. However, even before the beam radius, w_0, is reached, the parabolic profile approximation actually gives the wrong sign for the nonlinear index of refraction term. Referring to Fig. 7, which shows the same comparison extended out to a radius equal to $3w_0$, we again see that the parabolic approximation gives the wrong sign, and in addition gives a larger magnitude for the intensity than is found on axis. The result is that the focusing of a beam estimated from the parabolic approximation of self-focusing is greater than actually occurs in a nonlinear material.

An additional limitation that one finds in using the parabolic GRIN lens approximation of self-focusing is that this method is restricted to an approximation of the TEM_{00} mode. Higher order spatial modes have been reported [39] in KLM Ti:sapphire lasers, especially before modelocking occurs. Also, quite un-parabolic index profiles resulting from higher order spatial modes, which appear in the cavity due to intracavity aperture diffraction, can not be modelled well at all. Siegman [3] has shown that a circular aperture placed in the path of a TEM_{00} Gaussian mode such that only 1% of the power of the beam is blocked results in a 17% on axis intensity ripple in both the near and far field. Since many apertures used in practice in KLM Ti:sapphire lasers are designed to block more than 1% of the power of the beam in cw operation [11], this inability of the parabolic ABCD

method to approximate self-focusing in other than TEM_{00} mode distributions is another good reason to seek a more exact analysis of beam propagation in nonlinear media.

CHAPTER V

USE OF FOURIER TRANSFORM TO MODEL SELF-MODELOCKING

For a higher level of accuracy in modelling beam propagation in a nonlinear medium, one of the often used methods is called the split-step Fourier method, first used to examine the combination of self-focusing and diffraction in a high power laser beam propagating through air [40]. The method has since been used to examine many nonlinear propagation problems, including fiber optic pulse propagation [43] and unstable laser design [42].

There are two basic steps in this method:

1) linear propagation and
2) nonlinear phase correction.

The entire distance across which the beam is propagated is divided up into small, discrete linear propagation steps. In between each linear propagation step, the nonlinear phase correction step is performed. Fig. 8 shows graphically how a beam is numerically propagated using this method. The number of steps required to accurately model a nonlinear propagation depends on the nonlinear response term. One

often models a given nonlinear propagation problem using successively shorter and shorter discrete linear distances until the results converge to a given degree of accuracy.

Linear propagation of a field through a linear medium can be modelled using Huygens' integral in the Fresnel approximation as [3]

$$E_{Lin}(x,y,z_o+\Delta z)=\frac{i}{\Delta z\lambda_0}\int_{-\infty}^{\infty}\int E(x_0,y_0,z_0) \times \exp\left[-ik_0\frac{(x-x_0)^2+(y-y_0)^2}{2\Delta z}\right]dx_0dy_0 \qquad \text{(Eq. 17)}$$

where Δz is the distance parallel to the z-axis from the entrance plane at $z = z_0$ to the exit plane at $z = z_0 + \Delta z$. To this linear propagation term the nonlinear phase correction is applied as

$$E(x,y,z)=E_{Lin}(x,y,z)\exp\left[\frac{4i\pi n_2 I\Delta z}{\lambda_0}\right] \qquad \text{(Eq. 18)}$$

In the modelling of self-focusing in a Ti:sapphire laser, a digital method was sought to perform the Huygens' integral. However, it was soon realized that not all digital methods are equally useful. Keeping in mind that because of the Nyquest criteria, there is a minimum number of discrete points that one must include to retain a given amount of 'information' in the waveform [43], the question of estimating the computation power required to solve this nonlinear problem needed to be addressed.

Assume a square grid that contains N x N discrete samples. In order to perform the above double integral as a discrete summation, for each sample on the exit plane, $E(x_m, y_n, z_0 + \Delta z)$, a distance Δz from the input plane one would need to calculate N^2 complex exponentials. Since there are N^2 such points on the exit plane, the total number of such sums to be performed is N^4 for every step in the z direction. Even a relatively loose grid of N = 128 samples would require the summing of 128^4 = 268 million complex exponential for each discrete step of Δz in the linear propagation. Note that in the numerical modelling of the Ti:sapphire laser, for a moderate peak power (over 10 kW for highly nonlinear materials, and over 100 kW for Ti:sapphire) it was necessary to use a minimum of 25 discrete linear and nonlinear steps in order to converge, and to pass the wave form back and forth through the cavity 50-100 times to establish a stable mode. Use of a digital summation to perform Huygens' integral for the linear portion of the propagation would have required about 300 billion complex exponential calculations per point on the power vs aperture loss curve. This represents a prohibitively large amount of computer time, making the method useless for a research tool.

A much more efficient method was found that uses the a two-dimensional Fourier Transform, which can be calculated numerically using any number of public domain Fast Fourier

Transform (FFT) routines, to perform the integral [44][45]. Since the Huygens' integral is a convolution integral, it is possible to perform a convolution in the spatial domain as a multiplication in the spatial frequency domain[46]. Appendix C shows the derivation of the application of the Fourier transform to perform the linear portion of the split-step beam propagation through a nonlinear medium.

There are two very large savings in using a 2 dimensional Fourier transform (2DFFT) method when compared to that of a 2 dimensional convolution. The first is that a 1 dimensional Fourier transform can be performed digitally in a very efficient manner. According to Pratt [45], a 1 dimensional FFT of a sequence of N discrete samples can be performed in $N\log_2(N)$ steps, instead of the N^2 steps required for the single dimension convolution. Pratt states that the second great savings in computational effort is that a 2DFFT can be performed as a combination of 1 dimensional Fourier transforms. This means that a 2 dimensional FFT on a N x N size grid requires not N^4, as is the case in the 2 dimensional convolution, but only $2N^2\log_2(N)$. The saving in computational effort scales as

$$\text{comp. savings with 2D-FFT} = \frac{N^2}{2\log_2(N)} \qquad \text{(Eq. 18)}$$

For a N size of 128

$$N^4 = 268\times 10^6$$

$$2N^2\log_2(N) = 229\times 10^3$$

Thus, for a relatively small grid size, the savings in computational effort is on the order of 1000. Note that this savings becomes much greater if more numerical accuracy is required.

However, there are two important problems that were found with using the 2DFFT method directly to model laser cavities. The first was that something like one quarter of a million exponential sums per discrete step Δz was still a sufficiently larger number of calculations to perform, when 128 points were sufficient to accurately describe a given laser cavity. This problem was overcome by using a different transform, the Hankel transform, which will be examined in the following section.

The second problem was that for a laser cavity with any kind of focusing, 128 points in each dimension did not give sufficient accuracy. This is because the same grid size that describes a beam at a mirror or lens, where the beam is perhaps 1 mm in diameter, must be used to describe the beam in a very tightly focused region, such as in the laser rod, where the diameter was sometimes a tenth as wide. Therefore, when a 128 x 128 grid sufficiently described the beam at the focus, then 1024 x 1024 grid was need to describe the beam when at the mirror because of the larger area covered by the beam at the mirror. Note that most of the 1024 x 1024 samples at the mirror contain redundant information, if we assume a properly scaled 128 x 128 grid spaced further

apart is sufficient. Again, this meant that only the numerical solution to the problem of beam propagation, though numerically correct, was too slow to be useful as a research tool.

This second problem was solved by using a space transformation algorithm developed by Sziklas and Siegman [47] in their study of mode calculations in unstable resonators. Their solution was to 'bend' the spatial dimension z to conform with the expanding and contradicting beam. This can be accomplished by making a z' axis expand with the phase radius of the beam, R(z). Referring to Fig. 9, the optical field in normal spatial coordinates, E(x,y,z), can be transformed to an equivalent optical field in primed coordinates, Y(x',y',z'), as

$$Y(x',y',z') = z\exp\left[\frac{i\pi}{z\lambda}(x^2+y^2)\right]E(x,y,z) \qquad \text{(Eq. 19)}$$

where the conversion to prime coordinates is given by

$$x'(x,y) = (\alpha x/z) \qquad \text{(Eq. 20)}$$

$$y'(x,y) = (\alpha y/z) \qquad \text{(Eq. 21)}$$

$$z' = \frac{\alpha^2(z-z_0)}{zz_0} \qquad \text{(Eq. 22)}$$

where z_0 is input plane and α is an arbitrary scaling constant. It is convenient to set α to unity. Sziklas and Siegman show that the transformed equivalent field Y(x',y',z') also obeys the paraxial waveform equation. This means that the 2DFFT method can be used on the primed coor-

dinate field as well. In the study of self-focusing in a Ti:sapphire laser, when the primed coordinates were scaled such that beyond the confocal parameter, the z′ axis is parallel to the diverging angle of the beam, it was found that one can reduce the variation in beam diameter significantly. In this manner, the requirement for a 1024 x 1024 grid size was reduced to a 128 x 128 grid size in many cases. Nonetheless, the numerical model was still found to be too slow.

CHAPTER VI

USE OF HANKEL TRANSFORM TO MODEL SELF-MODELOCKING

For beam profiles that are radially symmetric, most of the information in a 2D grid sampling of the intracavity beam is redundant. A significant savings in computational effort can be made if, for radially symmetric beams, a 1D description is used that looks at the radial dimension, r, instead of dimensions x and y. A radially symmetric version of the 2D Fourier transform method is available based on the Hankel transform beam propagation method [48][49][50][51]. Appendix D summarizes the derivation of the Hankel transform beam propagation method in a nonlinear medium and shows and example program used in this study.

Using the Hankel transform split-step beam propagation method, just as in the case of the FFT version of the split-step beam propagation method, requires the linear and non-linear steps to be repeated many times to propagate the field through the nonlinear crystal. For accurate modelling of a 8 mm crystal used in this study, as many as 100 steps per pass through the crystal were used to ensure convergence. Propagation through the linear portions of the

diffraction at the aperture, was done using the Hankel transform and the space transformation algorithm of Sziklas and Siegman.

Similar to the method used by Fox and Li [52], an initial field distribution was propagated around the cavity until the field converged to a mode. The initial field distribution used was the TEM_{oo} Gaussian beam found by solving the linear (zero-power) cavity without an aperture. Using the Hankel transform beam propagation method, the initial field was sent through many round cavity round trips (between 25-200, depending on the strength of the nonlinearity) until a mode formed. Once a stable mode was established in the cavity, aperture loss per pass was calculated.

Two kinds of KLM laser cavities were analyzed. The first cavity studied was a standing wave KLM Ti:sapphire fs laser, the same cavity presented in Fig. 5. This is a fairly typical design, in which the Ti:sapphire crystal acts as both a gain medium and an intensity dependent lens. A ring cavity with an additional highly nonlinear self-focusing element was studied as well. In both cavities, the wavelength used was λ_0 = 800 nm, which is near the peak gain of Ti:sapphire.

Figure 10 shows the KLM ring laser simulated in the study. It is idealized in the sense that, of the two media, only the highly nonlinear crystal is explicitly modelled,

since the nonlinear refractive index of the gain medium is often one or two orders of magnitude less than that of the self-focusing element.

In the ring cavity, the radius of curvature of the two mirrors, M_1 and M_2, was 10 cm, and the distance between the two mirrors was 11.1 cm for a nonlinear crystal length of 8 mm. For shorter nonlinear crystal lengths, the distance between mirrors was varied to keep the linear beam waist the same (i.e., the optical distance between M_1 and M_2 is kept constant). The distance from mirror M_2 to the adjustable aperture was set to 25 cm. Note that many other aperture positions were simulated for this cavity, including 5, 10, 15, 20, 30, and 35 cm from mirror M_2. However, the 25 cm distance was found to have the optimum loss characteristics of the positions tried. The total round trip physical length of the ring laser was set to 1.11 m. This resulted in a waist radius between M_1 and M_2 (before self-focusing) of about 25 μm.

For the purposes of simulations of the ring cavity with an additional nonlinear element, the n_2 of the nonlinear material used was 537 x 10^{-20} m^2/W esu (which is the n_2 of CdS [53]). CdS is used here as an example only. There are many other strongly nonlinear materials (e.g.; ZnS, ZnSe, SF57 glass) to which this study applies equally well.

For both the standing wave and the ring laser cavities studied, the diameter of the aperture used was set so that the zero-power loss at the aperture was about 4%. For the results presented below, the aperture in the Ti:sapphire standing wave cavity was 1.7 mm in diameter, while the results presented for the ring cavity are those for an aperture diameter of 1.25 mm. The distance d1 on the ring cavity figure is the distance in mm from the mid-point of the two curve mirrors to the center of the nonlinear crystal. For a symmetric placement of the crystal, d1 = 0. A positive d1 indicates that the crystal was moved closer to M_2.

CHAPTER VII

NUMERICAL RESULTS AND DISCUSSION

Figure 11 shows the relation between aperture loss and instantaneous intracavity power for the linear cavity KLM Ti:sapphire laser studied in the numerical simulations using the Hankel transform beam propagation method. Note that these results are quite similar to those found by Chen and Wang [11]. An important difference is that the previous study by Chen and Wang did not examine the relation between loss and power beyond 100 kW intracavity peak power. This is not necessarily the maximum peak power seen in real KLM Ti:sapphire lasers, which can produce pulses with an intracavity pulse peak power of 5 MW [39]. When higher intracavity peak powers are taken into account, one finds that the relation between pulse peak power and aperture loss is hardly linear, as was found previously by Chen and Wang. Also, the relation between loss and power no longer resembles the saturable absorber dye loss vs. power relation [4]. Instead, as seen before in the simple Gaussian thin lens approximation, self-focusing initially narrows the beam radius seen at the aperture. But at very high intracavity powers, self-focusing actually results in a beam broadening,

and thus acts to limit the pulse narrowing process. For this particular example, minimum aperture loss is found at an intracavity peak power of approximately 450 kW.

Fig. 12 shows aperture loss vs. intracavity instantaneous power in the KLM ring cavity studied using the Hankel transform beam propagation method for a d_1 = 3 mm and a CdS crystal of 8 mm in length. For this particular crystal location, the initial slope of the loss vs. power curve is -1.0×10^{-5} W^{-1}, which is two orders of magnitude larger than that of the KLM laser that uses Ti:sapphire for a self-focusing element. For this particular example, the minimum loss power is 7 kW. From Fig. 12, it is clear that for this nonlinear crystal position, power higher than 7 kW results in higher aperture losses. For comparison, Fig. 12 also includes the results from the standing wave single crystal (8 mm in length) Ti:sapphire KLM cavity. Following the publication of the numerical results summarized in this report [23], Heately, Dunlop and Firth [24] have also reported a similar relation between aperture loss and intracavity power in their numerical study of a KLM ring laser with an additional highly nonlinear intracavity element, thus replicating the results presented here.

It is important to note that the numerical results presented in this report can be easily applied to other nonlinear materials, since the nonlinear medium reacts to the product of the nonlinear index of refraction and the

intensity of the field. Thus, by properly re-scaling the power axis, one can find the relation between power and aperture loss for any given nonlinear material of the same thickness in the cavities presented. For example, calculation of the relation between loss and power in a similar cavity that uses SF57 glass, which has a n_2 that is 1/25 that of CdS, is accomplished by multiplying the power of the values presented by 25. Thus, for the ring cavity presented in Fig. 12 and a d_1 = 3 mm using a SF57 glass sample of 8 mm in length, the minimum loss power would be 25 x 7 kW = 175 kW.

Fig. 13 shows a family of curves showing loss vs. power for the same KLM ring laser with d1 varied from 0 to 5 mm for a 8 mm length of CdS. Not shown in Fig. 13 is the loss vs. power curves for negative d1 values, since the simulations of such cavities showed aperture losses increasing with intracavity power so that the lowest loss was found to be at zero intracavity power. This implies that in such cavities, self-focusing would tend to work against mode-locking. The possibility that self-focusing, because of crystal positioning, can therefore act to prevent mode-locking has been reported previously by Chen and Wang [11]. As the distance from the waist to the center of the crystal, d_1, is moved from d_1 = 0 to d_1 = 3 mm, the magnitude of initial slope in the loss vs. power relation, γ, increases. For this particular cavity configuration,

positioning the crystal center at d_1 = 3 mm results in the largest magnitude for γ and the lowest losses. For d_1 > 3 mm, the magnitude of γ decreases and the curves become shallower. However, notice that the minimum loss power increases with increasing d_1. Moving d_1 from 2 mm to 4 mm results in the minimum loss power moving from 5.5 kW to 8.5 kW.

This shift in minimum loss power with changing d_1 is even more pronounced with a thinner (1 mm) CdS crystal. Fig. 14 shows a family of curves for the same ring cavity with a 1 mm thick CdS crystal. Note that symmetric positioning of the nonlinear crystal with respect to the waist of the beam gives higher losses for increased intracavity power. Again, for comparison purposes, the loss vs. power curve for standing wave 8 mm Ti:sapphire KLM laser is shown. As can be seen from Fig. 14, the steepest initial slope, γ, occurs when the center of the nonlinear crystal is placed 1.5 mm from the center of the waist. The parameter γ is then -2.33×10^{-6} W^{-1}, and the minimum loss power is about 25 kW. This results in a minimum aperture loss equal to 1.2%. When d_1 is increased to 2 mm, the minimum loss power increases to about 35 kW, while the minimum loss decreases to about 0.5%. Moving the crystal farther from the waist increases the minimum loss power and the minimum loss as well. Moving the crystal beyond 4 mm has little impact on the minimum loss power, but significantly increases the

losses at the aperture and the initial slope, γ. Thus, with a 1 mm piece of CdS as a self-focusing element, the minimum loss power can be varied from 18 kW to 70 kW by adjusting the crystal position.

The results of the numerical simulations can be interpreted as follows. First, note that a laser will tend to operate where gain is maximum. Assuming that the GVD of the intracavity laser pulse is compensated properly and the laser bandwidth is large enough, the above numerical results imply that the laser will tend to operate at a peak power corresponding to the minimum loss power. Under these conditions, the minimum loss power represents the operating point of the modelocked laser. This is because, as a modelocking mechanism, self-focusing can act to discriminate against the highest power pulses, thus prevent further pulse narrowing.

It is interesting to compare of the loss vs. power curve found in this report and that of the classic dye saturable absorber. Note that a dye saturable absorber, which the self-focusing mechanism is often modelled as [11] [20][54], has the ability to 'bleach' so that essentially no losses are experienced. The relation between input intensity, I, at a dye jet or cell and the absorption coefficient of the dye, γ, is given as [4]

$$\gamma = \frac{\gamma_o}{1 + (I/I_s)} \qquad \text{(Eq. 23)}$$

where γ_o is the absorption coefficient at zero intensity and I_s is the saturation intensity. Thus, setting the intensity to infinity results in zero absorption in an ideal dye saturable absorber.

However, the results presented here suggest that there may be no similar saturation effect in self-focusing modelocking. To the contrary, as the intensity of a given beam increases, so does the focusing power of the nonlinear lens. At an extremely high intensity (higher than that seen in a mode-locked KLM laser) the beam would experience self-trapping, where the beam diameter collapses and material damage results [55]. Up to this limit, the focusing power of the self-focusing element increases monotonically, without saturation. Thus, one might suspect, without going through the task of numerically simulating such a system, that one can not 'bleach' a self-focusing modelocking mechanism. As the numerical simulations described in this report have shown, the focusing power of the nonlinear lens simply increases. Initial beam narrowing at the aperture is, at high enough powers, followed by beam expansion, until the cavity becomes unstable. This instability was seen in the simulations when, for powers much higher than those presented in the figures, no stable mode was formed after 200 round trips through the cavity. Instead, the beam seem to oscillate between a high loss and a low loss 'mode'. Thus,

self-focusing modelocking represents a fundamentally new kind of mode-locking device, which does not operate like a classical saturable absorber.

As seen in Figs. 13 and 14, the minimum loss power of a KLM laser, and therefore its operating point, is adjustable. A given laser can be optimized to maximize γ, and thus maximize the probability of stable self-modelocked operation. This is especially important in a laser material that has a very wide gain bandwidth, but operates at a lower intracavity power than found in Ti:sapphire lasers. This suggests, for example, that self-modelocking in a diode pumped Cr:LiSAF laser is possible. Since different elements are responsible for the gain and self-focusing in a laser with a separate nonlinear focusing element, the position of the nonlinear element can be optimized without sacrificing gain. This feature gives an additional degree of freedom in designing a KLM laser, which can not be accomplished in a Ti:sapphire KLM laser where a single crystal performs both functions.

One will recall that in the statement of the problem, three particular goals for improvement in the current design of KLM Ti:sapphire lasers were listed:

1) lower pump power requirements for modelocked operation,

2) make a linear cavity KLM Ti:sapphire laser self-starting, and

3) improve the long term stability of the laser.

We have seen, based on the numerical simulations in the preceding sections, that the initial slope of the loss vs. power curve can be significantly increased by the addition of a highly nonlinear intracavity element to a KLM laser. This could be interpreted to suggest that the addition of a highly nonlinear element would make self-starting more likely, and that once modelocking is achieved, modelocking would be more stable.

The fact that the minimum loss power can be shifted to a much lower instantaneous power by the addition of a highly nonlinear material to the cavity was also seen. This suggests that modelocking can be achieved in a KLM Ti:sapphire laser with a significantly lower intracavity average power. This could be achieved by using higher output couplers, or by lower pump power, or some combination of both. The suggestion is that such a laser would produce femtosecond pulses with a lower peak power. Note that this is consistent with the view of the laser as a soliton-like (solitary) laser, as is the view of Krausz, et al. [17]. This can be seen by noting that for a soliton, pulse peak power and pulse width are related as [33]

$$P_0 = \frac{\kappa}{n_2 \tau_p^2} \qquad \text{(Eq. 24)}$$

where P_o is the pulse peak power of a first order soliton, n_2 is the nonlinear index of refraction of the medium, τ_p is

the pulse width and κ depends on the effective area of the optical field, GVD and the wavelength of the pulse. Similarly, an increase in the nonlinearity in a KLM laser cavity allows for a proportional decrease in the pulse peak power of soliton for a given pulse width. Note also from the numerical results that the effective nonlinearity of the cavity depends not only on nonlinear index of refraction of the materials used, by also on the position of these nonlinear materials with respect to aperture position and beam focus.

One question that the numerical model present above can not answer is: "What will occur in a modelocked KLM laser at higher intracavity average power?" One will note that beyond the minimum loss power, aperture loss increases for higher instantaneous power. Thus, we assume this is a regime that the laser does not operate, since a laser tends to run where losses are least. But, suppose we have aligned a given KLM laser such that it is operating at this minimum loss power and the power is then increased?

A possible result is that the pulse will broaden, so that the minimum pulse peak power still is equal to the minimum loss power for that particular cavity configuration. In light of the relation between soliton pulse power and pulse width, as presented above in equation Eq. 24, this would seem to be a reasonable result. Thus, increasing

power in a femtosecond modelocked KLM laser that is operating at the minimum loss power could result in pulses broadening to picosecond pulses.

Multi-pulsing has been observed in KLM lasers that are pumped too high [39]. Some researchers have interpreted these multi-pulses as evidence of higher order solitons in the laser [34]. However, the numerical model developed to investigate KLM modelocking presented in the above sections offers an alternative explanation to multi-pulsing in KLM Ti:sapphire lasers that are pumped too hard. Note that a higher-order soliton is a periodic waveform with a peak pulse power that exceeds the lowest order soliton pulse peak power at least once per soliton period [33]. However, the numerical study presented int this report would suggest that higher-order solitons may be prevented from occurring in a laser cavity where the minimum loss power is less than that required to form a higher order soliton. Thus, a soliton-like pulse travelling in a KLM laser may be split into two separate lower order solitons when pump power is increased, instead of a single higher order soliton. This would explain why the peak power from a multi-pulsing KLM laser is less than that of a single-pulsing KLM laser. However, since the power required for a higher order soliton depends on the GVD of a given cavity, this limitation may not apply to all cavities, and thus depends precisely on the cavity configuration.

CHAPTER VIII

EXPERIMENTAL LINEAR CAVITY KERR LENS MODELOCKED TI:SAPPHIRE LASER

Fig. 15 shows a schematic of the experimental Ti:sapphire laser used to test the effect of the addition of a highly nonlinear intracavity element in a KLM laser. Mirrors M_1, M_2, M_3, and M_4 had a radius of 10 cm. The center wavelength of the operating laser was 766 nm. Mirrors M_1 through M_4 were placed in mirror mounts that allowed two dimensional tilt adjustment. These mirror mounts were then placed on single dimension translation stages. The high reflectors, HR_1 and HR_2 were flat.

There were two output couplers tested in the experimental KLM laser. The Low Transmission Output Coupler (LTOC) had a 1.1% transmission, while the High Transmission Output Coupler (HTOC) had a 10% transmission. Both the LROC and the HROC were flat. The output couplers and the higher reflectors H_1 and H_2 were placed in tiltable mirror mounts and bolted onto fixed, low vibration 2 inch diameter pylons made in the ECEN machine shop here at OSU.

GVD corrections prisms, P_1 and P_2, were made of SF11 glass cut for minimum deviation at the Brewster angle. Appendix E shows the method used to calculate the zero GVD cavity position for these prisms, depending on the material being tested. The calculation is based on the method developed by Gordon, Fork, and Miller [21]. The distance was varied from 30 to 56 cm. These prisms are mounted on single dimension translation stages. Note that by moving prism P_1 out of the path of the cavity beam, HR_1 becomes the high reflector for the system. Conversely, when P_1 is placed in the path of the cavity beam, high reflector HR_2 is used. Thus, the laser can be used as either a cw Ti:sapphire laser when HR_1 is used, or as a modelocked KLM laser when HR_2 is used.

A Brewster cut 20 mm length Ti:sapphire rod was placed in the astigmatically corrected 'z' between mirrors M_1 and M_2. Appendix G shows the method as well as an example of the astigmatism correction calculations used. The figure of merit of the Ti:sapphire rod was greater than 250, where figure of merit for Ti:sapphire is defined as the ratio of the absorption coefficient at the central pump wavelength (approximately 514 nm) over the absorption coefficient at the center gain wavelength (approximately 800 nm [4]). The laser was end pumped through mirror M_1 by an argon ion laser using all available visible lines. The laser rod was set in an aluminium, water-cooled block with thermal compound used

to bring the surface of the Ti:sapphire rod into contact with the aluminium block designed and built by Czeslaw Radzewicz in the ECEN machine shop. The aluminium block was then mounted on a rotatable X-Y-Z translation stage for fine adjustment.

In the second 'z' (between mirrors M_3 and M_4) was where the nonlinear intracavity element was placed at a Brewster angle. The astigmatism correction angle, β, shown in the figure was adjusted to minimize astigmatism for the different types of nonlinear elements that were tested. The nonlinear element was mounted on a precise X-Y-Z translation stage for fine adjustment, since previous [11] as well as the numerical simulations presented in above sections had shown that the distance, d_1, from the focus to the center of the crystal, was a critical parameter for self-modelocking performance of the laser. When birefringent nonlinear elements were tested, it was necessary to mount them such that the cavity beam was polarized along only one axis of the nonlinear element. In one case, when a nonlinear glass, SF11, was tested, it was necessary to slowly rotate the sample such that the rotation axis of the glass sample was parallel to the plane of the optical table to eliminate the effects of thermal lensing. In the case of the crystals tested, this was not necessary.

The figure also shows a Slowly Modulated Brewster Plate (SMBP) which was used to modelock the laser. The technique of using a SMBP (also called a shaker [18]) is well established in the modelocking of Ti:sapphire KLM lasers. In this study it was used to modelock the laser in the absence of a nonlinear response strong enough to produce self-starting, as in the case of the Ti:sapphire laser without the additional nonlinear element, or to help align the laser for peak nonlinear response when the laser cavity included a highly nonlinear element. The SMBP was turned off when this alignment was found.

The aperture shown in the figure was a variable vertical slit aperture, with the slit perpendicular to the plane of the optical table upon which the laser was constructed. The aperture itself was used as an option, since often, as will be explained in the following section, the laser modelocked without this aperture in the system. The position of the aperture shown in the figure is that which was found to have the most impact, though other positions were tested. Note that in placing the aperture between the GVD correction prisms, the aperture could be moved such as to act as a wavelength tuner as well.

Output pulses were monitored by the use of an intensity autocorrelator. The autocorrelator, built by Czeslaw Radzewicz, used a thin piece of KDP and a slowly rocking retroreflector on one arm of a standard Michelson interferometer

to monitor pulse widths. The second harmonic generated signal was appropriately filtered to remove pump and cavity beams, and the output amplified by a PMT. The PMT amplified autocorrelator signal was then displayed on a digital storage scope, which could download the waveform displayed to a plotter for record keeping purposes. The digital scope was switched to operate in the x-y mode, where the sinewave (roughly 1 to 20 Hz) driving signal to the rocking retro-flector arm was used for the x input, and the output of the PTM was used as the y input. The duration of the autocorrelation pulse was calibrated by comparing the movement of one of the retro-reflectors on the autocorrelator interferometer arms with the movement of the waveform on the digital scope. By making one arm longer or shorter, the position of the autocorrelation pulse waveform is shifted in time. The ratio of the shift of the waveform on the digital scope to the distance the retro-reflector has been moved can then be used to create a time scale along the x axis. Note that the change in the distance the beam travels on one arm is twice the distance the retro-reflector is moved, since the beam is reflected back along the same path.

In addition to the autocorrelator, a cravat of R6G dye in solution, which does not absorb at 766 nm, was placed in a focused portion of the laser output. When the laser was modelocked, two-photon absorption in the dye allowed one to observe a strong fluorescence in the orange-yellow portion

of the spectrum. When the system was not modelocked, the dye did not fluoresce, since there was little light absorbed. Since this response was much faster than the autocorrelator waveform on the digital scope, this simple 'modelock detector' was often used to provide quick feedback when aligning the laser for strong modelocking output.

The nonlinear elements tested were made of SF11 glass, CdS, ZnSe, polycrystalline and monocrystalline ZnS, and cubic zirconia (CZ). The nonlinear index of refraction, n_2, of these materials is listed in Table 2. Appendix F shows the method used to calculate the n_2 of the materials. This method is based on an empirical relation found by Boling, et al. [56].

Table II

LINEAR AND NONLINEAR INDEX
OF REFRACTION

material	n_0	n_2 ($x10^{-20}$ m^2/W)
quartz	1.53	3.0
Ti:Al_2O_3	1.76	2.9
CZ	2.1	27.7
SF11	1.7	29.5
ZnS	2.29	90
ZnSe	2.7	383
CdS	2.34	537

For each nonlinear element, the angle β, is calculated to correct for astigmatism. For the control case (where no additional nonlinear element is contained in the laser cavity) the SMBP, made of quartz, was placed in the second 'z' between mirrors M_3 and M_4. Note that the nonlinear index of refraction of quartz is very close to that of Ti:sapphire, which is very small compared to the other materials. Thus, the nonlinear impact of the quartz on the laser is minimal, while the astigmatism is corrected. In this manner, such factors as loss due to the addition of mirrors M_3 and M_4 as

well as astigmatism are the same for the case where there is no additional highly nonlinear element in the cavity as well as for the cases where an additional highly nonlinear element was tested is used.

CHAPTER IX

TESTING OF THE EXPERIMENTAL TI:SAPPHIRE LASER

There was a particular output beam pattern that seemed to indicate that the cw laser was very close to modelocking. A rough sketch of this beam pattern is shown in Fig. 16. This pattern obviously contains higher order spatial modes, since it had such a definite structure. When this output beam mode was present, the laser could be brought into self-modelocking by slowly tilting the output coupler, or by moving mirror M_4 very slightly in closer to the center of the 'z'. When the laser switched from cw to modelocked operation, the output beam mode went from the one presented in Fig. 16 to one that is presented in Fig. 17. This is also a higher order mode, but it can be seen that the four circular portions of the cw mode located away from the center of the beam have disappeared. Although a complete analysis of the beam pattern was not performed, it would seem that the modelocked pattern had more power concentrated in the center of the beam compared to the cw pattern. This is consistent with the view that through self-focusing, the modelocked beam is focused through an intracavity aperture,

first discussed by Piche' [20]. Pulses produced from the modelocked laser ranged from 5 ps to 50 fs, depending on the position of the GVD prisms.

It was found that modelocking could be initiated without the vertical slit aperture in the cavity. In this case, the aperture in the laser that seemed to control modelocking was often the edge of prism P_2. Because the beam was directed through the upper portion (closest to the apex) of prisms P_1 and P_2, there was some amount of the beam that spilled over the edge, and was thus not directed towards HR_2. The path through the prisms was kept to a minimum in general to minimize chromatic dispersion. When laser alignment was such that the laser was very close to modelocking, there was a significant portion of the beam spilling over this edge, and was seen as a bright red dot against a screen set near prism P_2. Once modelocked, the beam path changed slightly so that the amount of light that spilled over the edge of prism P_2 was largely diminished, such that the bright red dot on the screen disappeared. This indicates that the prism edge could have been acting as a discriminator between cw and modelocked operation, with self-focusing re-directing the beam path to one that moves away from the apex of P_2 a small amount, thus reducing intracavity losses for this mode. Interestingly, Spence, et al. [1], note that a prism edge was also the discriminator in the first self-modelocked Ti:sapphire laser.

When the vertical slit aperture was used to modelock the laser, the change in beam path, which was so noticeable in the case of the prism edge acting as a modelocking discriminator, was impossible to monitor. However, using the vertical slit aperture was helpful in controlling a 'strobing' of the beam across the surfaces of prisms P_1 and P_2 due to thermal lensing from the prisms. Thus, the vertical slit, though not necessary to modelock the laser, made the output much more stable, in the sense that modelocking was less likely to switch off suddenly.

Testing of the linear cavity Ti:sapphire KLM laser was done to characterize KLM modelocking with and without an additional highly nonlinear intracavity element. The Ti:sapphire KLM laser was characterized in term of the following parameters:

1) minimum pump power required to sustain self-modelocking,

2) self-starting and

3) long-term stability of modelocked operation.

The following sections summarize the procedures used to characterize the laser in these terms and the results.

CHAPTER X

SELF-MODELOCKING PUMP POWER THRESHOLD RESULTS AND DISCUSSION

The search for the minimum power required to sustain self-modelocking was accomplished in the following manner. After the laser was warmed-up (which could take up to 30 minutes because of the warming time of the argon ion tube) the SMBP was engaged and the laser aligned until self-modelocking was seen to occur. Modelocking was monitored using a fast photodiode, a cravat of R6G dye, and the autocorrelator. Note that the procedure was begun at relatively high pump power (around 9 to 10 W) even in the case where highly nonlinear element was used.

Once the laser was aligned to produce a modelocked output with the SMBP turned on, the power was reduced slightly (in increments of roughly 0.1 W) and the SMBP turned off. If the laser remained modelocked, then it was considered to be sustaining self-modelocking. This was done to ensure that the modelocking mechanism was the optical Kerr effect alone, and not the shaking SMBP action itself. However, if the laser output did not remain modelocked after the SMBP was turned off, the SMBP was re-engaged, and the procedure repeated. The Self-Modelocking Pump Power Threshold (SMPPT)

for each laser cavity configuration was defined to be the lowest power at which the laser remained modelocked after the SMBP was switched off.

Table 3 summarizes the results of this comparison. The SMPPT is shown for the 1.1% output coupler and the 10% output coupler, as well as the n_2 of each material for the quartz SMBP, which is used as a control case, SF11 glass, cubic zirconia (CZ), monocrystalline ZnS and polycrystalline ZnS. Note that ZnSe (n_2 = 383 x 10^{-20} m^2/W) and CdS (n_2 = 537 x 10^{-20} m^2/W) were also tested. However, the laser was not successfully modelocked when these two very highly nonlinear materials were used.

As shown in the table, the Ti:sapphire KLM laser with the quartz (n_2 = 3.0 x 10^{-20} m^2/W) SMBP in the 'z' between M_3 and M_4 had a SMPPT of 5.4 W when the 10% output coupler was used, and 4.8 W when the 1.1% output coupler was used. Thus, by using an output coupler with a lower transmission, it is seen that the intracavity power is significantly raised. Thus, the laser could be modelocked with a lower pump power. The difference between the SMPPT for the different output couplers is as expected, since we assume that the self-modelocking power threshold is based on the intracavity power, not the pump power *per se*.

This compares with the Ti:sapphire laser when a 3.75 mm thick piece of monocrystalline ZnS (n_2 = 90 x 10^{-20} m^2/W) was placed in the cavity. When the 10% output coupler was

used, the laser with monocrystalline ZnS had a SMPPT of 3.7 W. When the 1.1% output coupler was used, the SMPPT dropped to 2.3 W. It should be noted that the lasing threshold of the laser increased from 1.8 W to 2.1 W when the monocrystalline ZnS was added to the cavity compared to when the quartz SMBP was placed in the second 'z'. Thus, for both output couplers, the SMPPT of the laser was significantly lowered when the additional nonlinear element was added to the cavity, even though the ZnS crystal added more linear loss to the system.

The results obtained from other nonlinear elements tested show a relation between the SMPPT and the n_2 of the material for each of the two different output couplers. For example, using a sample of SF11 glass ($n_2 = 30 \times 10^{-20}$ m^2/W) in the second 'z' resulted in a SMPPT that was between that of the monocrystalline ZnS sample and that of quartz. However, losses in the crystal due to two-photon absorption resulted in a higher than expected SMPPT for CZ ($n_2 = 28 \times 10^{-20}$ m^2/W) and for polycrystalline ZnS. When CZ was used in the cavity, modelocking occurred simultaneously with a bright green fluorescence in the CZ crystal. In the case of the polycrystalline ZnS, there was a bright purple glow from the crystal when the system became modelocked. Thus, it would seem that two-photon absorption in these crystals worked to raise the SMPPT of the laser when the laser was modelocked.

Table III

SELF-MODELOCKING PUMP POWER THRESHOLD

material	SMPPT (1%)	SMPPT (10%)	n_2 (10^{-20} m^2/W)
quartz	4.8 W	5.4 W	3.0
SF11 glass	3.0 W	4.3 W	29.5
CZ	3.4 W	4.7 W	27.7
ZnS (m)	2.3 W	3.7 W	90
ZnS (p)	2.5 W	4.1 W	90

CHAPTER XI

SELF-STARTING RESULTS AND DISCUSSION

The experimental Ti:sapphire KLM laser built was tested for self-starting with and without an additional highly nonlinear self-focusing element. The test for self-starting was done after the laser was aligned as explained above and without the SMBP engaged. A card was used as a beam block in the cavity between M_3 and the output coupler. If the laser returned to modelocked operation without re-engaging the SMBP or table banging (essentially a cruder but similar technique) the laser was then said to be self-starting. Consistent self-starting implies that out of a large number of trials, the laser returned to modelocked operation in a reasonable length of time each time.

Without an additional nonlinear element in the cavity, the results were very similar to that of previous researchers [1]. The Ti:sapphire laser without an additional nonlinear element in the laser would only occasionally self-start. When monocrystalline ZnS was used as the additional nonlinear element, the laser was found to self-start consistently. This would seem to be the first linear cavity KLM Ti:sapphire laser that self-starts using self-modelocking alone reported.

The self-staring response of the laser seemed to depend on the pump power in the following manner. For a rather high pump power of 5.6 W and using the 10% output coupler with monocrystalline ZnS used as a modelocking element, the laser self-started in less than a second 50 times out of 50 trials. When the pump power was reduced to 4.6 W, the laser also self-started consistently, but the delay from the time the card was removed and the laser began to modelock was often more than a second. When the pump power was reduced further to 4.2 W, it was seen that the laser self-started roughly half of the time if one waited for up to a few seconds.

Self-starting was also observed when CZ was used as a self-focusing element as well. For example, when the laser was seen to consistently self-start when it was pumped with 5.3 W, using the 1.1% output coupler and CZ as the self-focusing element.

These results seem to imply that self-starting should be viewed as a random event. Thus, the highly nonlinear cavity created when the monocrystalline ZnS was placed in the cavity makes it more likely that some random fluctuation in the intracavity beam power distribution would be large enough to eventually force the laser into modelocked operation. The intracavity instantaneous power threshold required to modelock the laser is lowered when the cavity as a whole is made more nonlinear. As the pump power is reduced, the size of

the intracavity beam power spike required to overcome the various losses and back-scattering working against modelocking may well remain the same. But such an event becomes less likely when the average intracavity beam power decreases. Thus, as pump power is reduced, there is often a longer delay before the laser self-starts.

Compare this to the case when there is no additional nonlinear element in the cavity. Now, it would seem that the self-starting threshold has been significantly increased, since at all pump powers tried (up to 12 W) modelocking in the laser without the additional nonlinear element was only very occasionally self-starting. Thus, it might be that the peak instantaneous power required to self-start modelocking operation in the laser may indeed be quite large, since it seems that this event was very rare. However, since there was no way to actually monitor the instantaneous intracavity beam distribution on a femtosecond time scale, this interpretation nonetheless remains somewhat speculative.

CHAPTER XII

STABILITY RESULTS AND DISCUSSION

Comparison of the stability of the Ti:sapphire KLM laser with and without an additional nonlinear modelocking element was tested. The laser was first modelocked, and the SMBP was turned off. The length of time the laser remained modelocked was observed. It was found that the laser, when no additional nonlinear element was included in the cavity, would often remain modelocked for periods up to about one half hour, but not beyond that time. This is consistent, again, to the findings of other researchers [1] who report that modelocking would remain unassisted for a short period of time if the laser was left undisturbed (no table banging or mirrors tapped).

When the laser was tested with the intracavity monocrystalline ZnS element, modelocked was maintained without assistance for longer periods of time. One test of stability showed that the laser remained modelocked for 12 hours, at which point the laser was shut down due to the fatigue of the researcher. Thus, the additional ZnS element made the laser significantly more stable.

These results might best be interpreted by assuming that switching from modelocked to cw operation requires some disturbance threshold which is dependent on the nonlinearity of the cavity. The higher the nonlinearity, the higher the disturbance threshold becomes. Small vibrations present in the system, through shaking equipment, water pumping vibrations, fluctuations in the argon ion laser focusing and output power, or dust particles passing through the pump and the cavity beam, all could act as small, temporary, 'beam blocks', either complete or partial. It the disturbance threshold is raised by increasing the nonlinearity of the laser, and if large disturbances are less likely than small ones, the likelihood of disturbance large enough to surpass this threshold is decreased.

Additionally, if the laser is designed such that modelocking is self-starting, then the system will readily recover from such temporary interruptions without detection, even when disturbance threshold is exceeded. This may have been the case when monocrystalline ZnS was in the cavity. We have already seen that this makes self-starting much more likely. However, if the nonlinearity of the laser is not strong enough to make modelocking self-starting, then a brief interruption in the operation of the laser, if long and complete enough, could easily end modelocking operation completely. Again, this seems to be the case when Ti:sapphire alone is used as a self-focusing modelocking element.

CHAPTER XIII

CONCLUSIONS

Numerical simulations of the relation between aperture loss and intracavity instantaneous power in standing wave and ring cavities show that the combination of self-focusing and aperture loss used as a modelocking mechanism is a different sort of passive modelocking mechanism than a saturable absorber dye. This is the case in both single crystal and two crystal KLM lasers, and was seen in both standing wave and ring laser cavities as well. Thus, along with SPM, GVD, gain bandwidth, and the bandwidth of the cavity mirrors used in lasers, self-focusing can act as a limiting factor on achievable pulse widths in ps and fs KLM lasers. The minimum loss intracavity power in a KLM laser, first established here at the OSU Laser Center, is observable in a running KLM laser as multi-pulsing. Thus, a better understanding of KLM modelocking has been achieved.

This report also has summarized experiments done here at the OSU laser Center on a linear cavity KLM Ti:sapphire laser with an additional highly nonlinear intracavity self-focusing element. By the addition of monocrystalline ZnS, for example, it is possible to:

1) lower pump power requirements for sustained self-modelocked operation,

2) make a linear cavity Ti:sapphire KLM laser self-starting, and

3) improve the long term stability of the laser.

The method has led to development at the OSU Laser Center of the first known consistently self-starting linear cavity KLM Ti:sapphire.

REFERENCES

1. D. E. Spence, P. N. Kean, and W. Sibbett, Optics Lett., **16**, 42 (1991).

2. C. Huang, M. T. Asaki, S. Backus, M. M. Murnane, H. C. Kapteyn, and H. Nathel, Optics Lett., **17**, 1289 (1992).

3. A. E. Siegman, Lasers, University Science Books, Mill Valley, California (1986).

4. W. Koechner, Solid-State Laser Engineering, 2nd. ed., Springer-Verlag, Berlin (1998).

5. Q. Fu, G. Mak, and H. M. van Driel, Optics Lett., **17**, 1006 (1992).

6. W. S. Pelouch, P. E. Powers, and C. L. Tang, Optics Lett., **17**, 1070 (1992).

7. C. Rouyer, E. Mazatahd, I. Allais, A. Pierre, S. Seznec, C. Sauteret, G. Mourou, and A. Migus, Optics Lett., **18**, 214 (1993).

8. W. E. White, J. R. Hunter, L. van Woerkom, T. Ditmire, and M. D. Perry, Optics Lett. **17**, 1067 (1992).

9. W. H. Knox, Optics & Photonics News, **May**, 10 (1992).

10. K. Tamura, J. Jacobson, E. P. Ippen, H. A. Haus, and J. G. Fujimoto, Optics Lett., **18**, 220 (1993).

11. S. Chen and J. Wang, Optics Lett., **16**, 1689 (1991).

12. N. H. Rizivi, P. M. French, and J. R. Taylor, Optics Lett., **17**, 279 (1992).

13. W. S. Pelouch, P. E. Powers, and C. L. Tang, Optics Lett., **17**, 1581 (1992).

14. D. E. Spence, J. M. Evans, W. E. Sleat, and W. Sibbett, Optics Lett., **16**, 1762 (1991).

15. U. Keller, G. W. 'tHooft, W. H. Knox, and J. E. Cunningham, Optics Lett., **16**, 1022 (1991).

16. G. R. Jacobovitz-Veselka and U. Keller, Optics Lett., **17**, 1791 (1992).

17. F. Krausz, Ch. Spielmann, T. Brabec, E. Winter, and A. Schmidt, Optics Lett., **17**, 204 (1992).

18. Y. M. Liu, K. W. Sum, P. R. Prucnal, and S. A. Lyon, Optics Lett., **17**, 1219 (1992).

19. F. Salin, J. Squier, and M. Piche', Optics Lett., **16**, 1674 (1991).

20. M. Piche', Optics Comm., **86**, 156 (1991).

21. G. P. Malcolm and A. I. Ferguson, Optics Lett., **16**, 1967 (1991).

22. R. L. Fork, O. E. Martinez, and J. P. Gordon, Optics Lett., **9**, 150 (1984).

23. G. W. Pearson, C. Radzewicz, and J. S. Krasinski, Optics Comm, **94**, 221 (1992).

24. D. R. Heatley, A. M. Dunlop, and W. J. Firth, Optics Lett., **18**, 170 (1993).

25. C. Radzewicz, G. W. Pearson, and J. S. Krasinski, submitted to Optics Comm.

26. A. Hariharan, personal conversation. Hariharan, of Allied Signal, states that the of monocrystalline ZnS to a linear cavity KLM Ti:sapphire laser reduced the self-modelocking threshold from 3.5 W to 1.8 W.

27. R. Scheps, Optics Mater., **1**, 1 (1992).

28. N. H. Rizvi, P. M. French, and J. R. Taylor, Optics Lett., **17**, 1605 (1992).

29. V. E. Zakharov and A. B. Shabat, Soviet Phys. JETP, **34**, 62 (1972).

30. M. Schwartz, Information Transmission, Modulation, and Noise: a Unified Approach to Communication Systems, 3rd ed., McGraw-Hill Book Co., New York (1980).

31. Ch. Spielmann, P. F. Curely, T. Barbec, E. Winter and F. Krausz, Electron. Lett., **28**, 1532 (1992).

32. B. Procotor and F. Wise, Optics Lett., **17**, 1295 (1295).

33. G. P. Agrawal, Nonlinear Fiber Optics, Academic Press, Inc., Boston, (1989).

34. T. Tang, Optics Lett., **18**, 293 (1993).

35. M. J. Weber, D. Milam, and W. L. Smith, Optical Engineering, **17**, 463 (1978).

36. J. T. Verdeyen, Laser Electronics, Prentice-Hall, Englewood Cliffs, New Jesery (1981).

37. D. Huang, M. Ulman, L. H. Acioli, H. A. Haus, and J. G. Fujimoto, Optics Lett., **17**, 511 (1992).

38. D. Georgiev, J. Herrmann, and U. Stamm, Optics Comm., **92**, 368 (1992).

39. B. E. Lemoff and C. P. Bartey, Optics Lett., **17**, 1367 (1992).

40. M. D. Feit and J. A. Fleck, Appl. Opt., **17**, 3990 (1978).

41. G. P. Agrawal and M. J. Potasek, Phys. Rev. A, **33**, 1765 (1986).

42. E. A. Sziklas and A. E. Siegman, Appl. Opt., **14**, 678 (1975).

43. A. V. Oppenheim and R. W. Schafer, Digital Signal Processing, Prentice-Hall, Inc., Englewood Cliffs, New Jersey (1975).

44. W. H. Press, B. P. Flannery, S. A. Teukolsky, and W. T. Vetterling, Numerical Recipies, Cambridge University Press, New York (1986).

45. W. K. Pratt, Digital Image Processing, John Wiley & Sons, New York (1978).

46. C. M. Close and D. K. Fredick, Modelling and Analysis of Dynamic Systems, Houghton Mifflin Co., Boston (1978).

47. E. A. Sziklas and A. E. Siegman, Appl. Opt., **14**, 1874 (1975).

48. A. E. Siegman, Optics Lett., **1**, 13 (1977).

49. G. P. Agrawal, Optics Lett., **6**, 171 (1981).

50. M. Lax, J. H. Batteh, and G. P. Agrawal, J. Appl. Phys., **52**, 109 (1981).

51. S. Sheng and A. E. Siegman, Phys. Rev. A, **21**, 21 (1980).

52. A. G. Fox and T. Li, Bell System Tech. Journ., 453 (1961).

53. R. Adair, L. L. Chase, and S. A. Payne, Phys. Rev. B, **39**, 3337 (1989).

54. H. A. Haus, J. G. Fujimoto, and E. P. Ippen, IEEE Journ of Quant. Elec., **QE-28**, 2086 (1992).

55. P. L. Kelly, Phys. Rev. Lett., **15**, 1005 (1965).

56. N. L. Boling, A. J. Glass, and A. Owyoung, IEEE Journ. of Quant. Elect., **QE-14**, 601 (1978).

57. A. H. Cherin, An Introduction to Optical Fibers, McGraw-Hill Book Co., New York (1983).

58. A. Yariv, Quantum Electronics, 3rd ed., John Wiley & Sons, New York (1989).

59. M. J. Weber, CRC: Handbook of Laser Science and Technology, vol. III, CRC Press, Inc., Boca Raton, Florida, 203 (1986).

60. H. W. Kogelnik, E. P. Ippen, A. Dienes, and C. V. Shank, IEEE Journ. of Quant. Elect., **QE-8**, 373 (1972).

APPENDIX A

LINEAR LOSS MODELOCKING

MODEL PROGRAM

The following is an example program which simulates the modelocking of an initially un-modelocked intracavity beam. The program starts by filling the time samples array x with random values between 0.0 and 100 W. The zero power loss parameter b = 10%. The power dependent loss parameter a = -1×10^{-4} W^{-1}. Gain is accomplished as a simple re-normalization. This program is run for 50,000 'passes' through the cavity, and results in a single-modelocked output.

```
c      modelock.f - simulates modelocking using a linear
loss rule
c       implicit none
       parameter (N=4096)
       real*8 x,a,b,loss,norm,norm_orig,gain
       dimension x(N)
       integer seed,i,j,steps

       steps = 50e3
       seed = 13457
       OPEN(UNIT=10,FILE='modestart2',STATUS='UNKNOWN')
       REWIND(10)
       OPEN(UNIT=11,FILE='modeend3',STATUS='UNKNOWN')
       REWIND(11)
       do 100 i=1,N
         x(i) = 100.0*rand(seed)
         norm_orig = norm_orig + x(i)*x(i)
         write(10,*) x(i)
100    continue
```

```
      b = 0.1
      a = -1e-4
      write(*,*) ' '
      write(*,*) 'begin linear loss'
      write(*,*) ' '
      do 500 j=1,steps
        norm = 0.0
        do 300 i=1,N
           loss = a*x(i) + b
           if ( loss .LT. 0.0) then
              loss = 0.0
           endif
c           write(*,*) 'loss=',loss
           x(i) = x(i) - loss*x(i)
           norm = norm + x(i)*x(i)
300     continue
        gain = sqrt(norm_orig/norm)
        norm = 0.0
        do 400 i=1,N
           x(i) = x(i)*gain
           norm = norm + x(i)*x(i)
400     continue
500   continue

      do 600 i=1,N
         write(11,*) x(i)
600   continue
      CLOSE(10)
      CLOSE(11)
      end
```

APPENDIX B

DERIVATION OF PARABOLIC APPROXIMATION OF SELF-FOCUSING LENS

If we assume a TEM_{00} Gaussian distribution, then the intensity of a field, I(r,z), is [36]

$$I(r,z) = I_0 \exp\left\{-2\frac{r^2}{w^2(z)}\right\} \qquad \text{(Eq. B.1)}$$

A Taylor's expansion of the exponential function produces

$$e^{-x} = 1 - x + \frac{1}{2}x^2 \cdots \qquad \text{(Eq. B.2)}$$

so that

$$I(r,z) = I_0\left\{1 - \alpha + \frac{1}{2}\alpha^2 + \cdots\right\} \qquad \text{(Eq. B.3)}$$

$$\cong I_0\{1-\alpha\}$$

for

$$\alpha = 2\frac{r^2}{w^2(z)} \qquad \text{(Eq. B.4)}$$

The relation between intensity, I, and radius, r, is modelled as

$$I(r,z) = I_0\left\{1 - 2\frac{r^2}{w^2(z)}\right\} \qquad \text{(Eq. B.5)}$$

For a nonlinear index of refraction, n_2, the relation between index of refraction, n, and radius, r, is then approximated for a Gaussian pulse as

$$n(r) = n_o + n_2 I_0 \left\{ 1 - 2\frac{r^2}{w^2(z)} \right\} \qquad \text{(Eq. B.6)}$$

$$= (n_o + n_2 I_0) \left\{ 1 - \frac{2n_2 I_0}{(n_0 + n_2 I_0) w^2(z)} r^2 \right\} \qquad \text{(Eq. B.7)}$$

For a lens of thickness d with a parabolic index of refraction profile that varies as

$$n(r) = n' \left(1 - \frac{r^2}{2\beta^2} \right) \qquad \text{(Eq. B.8)}$$

the ABCD matrix is [36]

$$L_P = \begin{bmatrix} \cos\left(\frac{d}{\beta}\right) & \beta \sin\left(\frac{d}{\beta}\right) \\ -\frac{1}{\beta}\sin\left(\frac{d}{\beta}\right) & \cos\left(\frac{d}{\beta}\right) \end{bmatrix} \qquad \text{(Eq. B.9)}$$

where for $\beta = \infty$ the index of refraction is homogeneous.

For the self-focusing lens using the parabolic approximation,

$$n' = n_0 + n_2 I_0 \qquad \text{(Eq. B.10)}$$

$$\beta = \frac{w(z)}{2} \sqrt{\frac{n_0 + n_2 I_0}{n_2 I_0}} \qquad \text{(Eq. B.11)}$$

The following program is written in C++. It is an example of a program that uses the parabolic approximation to model self-focusing in a laser. The program uses the ABCD ray matrix approach to propagate a Gaussian beam through a 2 cm length of Ti:sapphire. Note that the E field is propagated, and thus the n_2 used is in units of m^2/V^2. For this

example, n_o = 1.76 and n_2 = 1.22 x 10^{-22} m^2/V^2, λ_o = 500 nm, peak pulse power is 80 kW, and waist size is 40 μm. The waist is assumed to be in the center of the 2 cm long crystal.

The routine 'main' is used to set the complex beam parameter, q, based on initialized values stated above and then to call a function 'nonlin'. The function 'nonlin' uses the parabolic GRIN lens approximation for propagation of the complex beam parameter, q, through the 2 cm length of Ti:sapphire in 2048 increments. The resulting beam diameter for each step for the linear and nonlinear propagation of q are both stored for comparison.

Functions 'input_data', which is commented out in the example below, allow data to be input from the screen for a laser cavity containing linear mirrors, free-spaces, and lenses as well. The function 'stab_check', also commented out in the example below, checks to make sure the linear cavity that data inputed in the 'input_data' routine results in a stable linear cavity. The function call to screen_fix sets the screen to allow the results to be displayed on a standard VGA screen for graphical viewing of beam changes.

```
#include <stdlib.h>
#include <graphics.h>
#include <dos.h>
#include <stdio.h>
#include <conio.h>
#include <math.h>
#include <time.h>
#include <complex.h>
FILE *in_file, *out_file, *stream;
int steps,check;
double m1[2][2], m2[2][2], m3[2][2],
```

```
      WW1[2048],WW2[2048];
complex q_lin,q_nonlin,qp,i(0,1);
double del_z,z,z0,w0,R,Rz,Rf,wz,wzf,zf,zf1,
      E0,E0_2,E0_2w0_2,n0,n2,l0,c,pi,d,gamma,some,lz;
double MM[2][2][11];
double A,B,C,D,stab;
double d1,d2,d3,f1,f2,l;
double nonlin(void);
double input_data(void);
double stab_check(void);
double screen_fix(void);
double P,P0, Pcr, P_Pcr,zfd,zfn,P_P0;
double max_mult(double m1[2][2],double m2[2][2],double
m3[2][2]);
main(){
  int j,k;
  pi = 4.0*atan(1.0);
  lz = 0.02;                    /* crystal length is 2 cm
*/
  n0 = 1.75;                    /* linear index of
refraction              */
  n2 = 1.6e-22;                 /* nonlinear index of
refraction MKS units */
  l0 = 500.0e-9;                /* wavelength in MKS
*/
  P  = 0.8e5;                   /* average pulse power
*/
  E0_2w0_2 = P*4*1.26*300/pi;
  z = -0.01;
  w0 = 40e-6;
  E0 = sqrt(E0_2w0_2/w0/w0);
  z0 = pi * w0 * w0 / l0;
  gamma = 4.0*n2*E0_2w0_2/n0;
  d = 2*sqrt(z*z);
  wz = sqrt(w0*w0*(1.0+z*z/z0/z0));
  R = z*(1.0 + z0*z0/z/z);
  q_lin = q_nonlin = 1.0/complex(1.0/R,-l0/pi/wz/wz);
  steps = 2048;
  del_z = d/steps;
  /*input_data();
  stab_check();*/
  check = nonlin();
  screen_fix();
  setcolor(2);
  settextstyle(0,0,1);
  outtextxy(520,460,"end of process");
  getch();
  closegraph();
  return(0);
  } /* end main */
```

```
/*******************************************************/
double input_data(void){
  int j,k;
  for(j=0; j<=9; j++){
      MM[0][0][j] = 1.0;
      MM[0][1][j] = 0.0;
      MM[1][0][j] = 0.0;
      MM[1][1][j] = 1.0;
      }
  MM[1][1][2] = 1.0/n0;          /* propagation from space
to crystal */
  MM[1][1][4] = n0;              /* propagation from crystal
to space */
  /*printf("what is f1 ?  ");
  scanf("%lf",&f1);*/
  f1 = 0.1/2.;                   /* R1 = 10 cm */
  MM[1][0][0] = -1.0/f1;         /* M1 mirror matrix */
  /*printf("what is f2 ?  ");
  scanf("%lf",&f2);*/
  f2 = 0.1/2.;                   /* R2 = 10 cm */
  MM[1][0][6] = -1.0/f2;         /* M2 mirror matrix */
  /*printf("what is d1 ?  ");
  scanf("%lf",&d1);*/
  d1 = 0.105;                     /* d1 = 10.5 cm */
  MM[0][1][1] = d1;               /* distance from M1 to
crystal */
  /*printf("what is d2 ?  ");
  scanf("%lf",&d2);*/
  d2 = 0.105;                     /* d2 = 10.5 cm */
  MM[0][1][5] = d2;               /* distance from crystal
to mirror M2 */
  /*printf("what is d3 ?  ");
  scanf("%lf",&d3);*/
  d3 = 0.5;                       /* d3 is half a meter */
  MM[0][1][7] = 2.0*d3;           /* distance from M2 to
flat mirror */
  /*printf("what is l ?  ");
  scanf("%lf",&l);*/
  l = 0.02;                       /* l = 2 cm */
  MM[0][1][3] = l;                /* length of crystal */
  for(j=0; j<=7; j++){
      printf("MM[0][0][%d]=%lf\tMM[0][1][%d]=%lf\n",j,MM[0][
0][j],j,
         MM[0][1][j]);
      printf("MM[1][0][%d]=%lf\tMM[1][1][%d]=%lf\n",j,MM[1][
0][j],j,
         MM[1][1][j]);
      }
  return(0);
  }/* end of input_data */
```

```
 /************************************************/
 double nonlin(void){
 int j;
 double zz;
 q_lin = q_lin*n0; /* change at medium boundry */
 q_nonlin = q_nonlin * n0;
 zz = 0.0;
 for(j=0; j<steps; j++){
    z = z + del_z;
    zz += del_z;
    if (zz > lz) return(0); /* check to see if we ran over
crystal len */
    q_lin = q_lin + del_z;
    q_nonlin = q_nonlin + del_z;
    some = -imag(1.0/q_nonlin);
    wz = sqrt(10/pi/some/n0);
    WW1[j] = wz;
    q_nonlin = 1.0/(1.0/q_nonlin - gamma*del_z/wz/wz/wz/wz);
    some = -imag(1.0/q_lin);
    WW2[j] = sqrt(10/pi/some/n0);
    }
 return(0);
 } /* end nonlin() */
/*****************************************************/
double max_mult(mm1,mm2,mm3)              /* 2x2 matrix mult
*/
double mm1[2][2],mm2[2][2],mm3[2][2];
{
int i,j;
      mm3[0][0] = mm1[0][0]*mm2[0][0] + mm1[0][1]*mm2[1][0];
      mm3[0][1] = mm1[0][0]*mm2[0][1] + mm1[0][1]*mm2[1][1];
      mm3[1][0] = mm1[1][0]*mm2[0][0] + mm1[1][1]*mm2[1][0];
      mm3[1][1] = mm1[1][0]*mm2[0][1] + mm1[1][1]*mm2[1][1];
      return(1);
}
/*****************************************************/
double stab_check(void){
   /* start at the surface of mirror one, and find the
round-trip
      matrix for this cavity
*/
   int j,k,l;
   m2[0][0] = 1.0;
   m2[0][1] = 0.0;
   m2[1][1] = 0.0;
   m2[1][1] = 1.0;
   for(j=1; j<=7; j++){
       printf("j=%d\n",j);
       m1[0][0] = MM[0][0][j];
       m1[0][1] = MM[0][1][j];
       m1[1][0] = MM[1][0][j];
       m1[1][1] = MM[1][1][j];
       max_mult(m2,m1,m3);
```

```
        for(k=0; k<=1; k++){
        for(l=0; l<=1; l++){
            m2[k][l]=m3[k][l];
            }
        }
        }
for(j=6; j>=0; j--){
   printf("j= %d\n",j);
        m1[0][0] = MM[0][0][j];
        m1[0][1] = MM[0][1][j];
        m1[1][0] = MM[1][0][j];
        m1[1][1] = MM[1][1][j];
        max_mult(m2,m1,m3);
        for(k=0; k<=1; k++){
        for(l=0; l<=1; l++){
            m2[k][l]=m3[k][l];
            }
        }
        }
   A = m2[0][0];
   B = m2[0][1];
   C = m2[1][0];
   D = m2[1][1];
   printf("A= %lf\t B= %lf\n",A,B);
   printf("C= %lf\t D= %lf\n",C,D);
   stab = (A+D)/2;
   printf("\n\tstab = %f",stab);
   if ((stab > -1.0) && (stab < 1.0)) {
      printf("\tcavity stable\n");
      return(1);
      }
   else{
     printf("\tThis is an unstable cavity\n");
     return(-1);
     }
} /* end stab_check()*/
/*************************************************/
double screen_fix(void){
char key[80],label[80];
int gdriver = DETECT, gmode, errorcode;
int xcenter,ycenter;
long j,jj,offset,N;
int x,y;
double ymax,ymin,ylen,yscale,xscale,tscale,P_m;
initgraph(&gdriver, &gmode, "c:\\borlandc\\bgi");
errorcode = graphresult();
if (errorcode != grOk){
   printf("graphics error: %s\n", grapherrormsg(errorcode));
   printf("press any key to halt:");
   getch();
   exit(1);
   }
rectangle(20,40,620,440);
```

```
offset = 00;
N=steps;
sprintf(label,"N = %ld  offset = %ld",N,offset);
outtextxy(10,10,label);
xscale = 600.0/N;
ymax=ymin=WW2[offset];
/*sprintf(label,"WW2[%ld] = %e ymax = %e",offset,WW2[off-
set],ymax);
outtextxy(10,20,label);*/
jj = 10;
for(j=offset;j<(offset+N); j++){
    if (WW2[j] > ymax) ymax = WW2[j];
    if (WW2[j] < ymin) ymin = WW2[j];
    }
yscale = 400./200e-6;
P_m = P/(pi*w0*w0)*1e-4;
sprintf(label,"power/cm2 = %e",P_m);
outtextxy(40,50,label);
sprintf(label,"E0 = %e V/m",E0);
outtextxy(40,70,label);
sprintf(label,"w0 = %e microns",w0*1e6);
outtextxy(40,90,label);
sprintf(label,"P = %e W",P);
outtextxy(40,110,label);
jj = 0;
setcolor(6);
moveto(20,440);
for(j=offset;j<(offset+N);j++){
    x= jj*xscale+20;
    y= 440.0 - yscale*WW2[j];
    /*sprintf(label,"y=%e",y);
    outtextxy(100,10+jj,label);
    sprintf(label,"WW2[%ld] = %e x=%d y=%d",j,WW2[j],x,y);
    outtextxy(10,20+jj,label);*/
    jj ++;
    lineto(x,y);
    }
moveto(20,440);
setcolor(4);
jj = 0;
for(j=offset;j<offset+N;j++){
    x= jj*xscale+20;
    y= 440-yscale*WW1[j];
    lineto(x,y);
    jj ++;
    }
return(1);
} /* end screen_fix() */
/***************************/
```

APPENDIX C

DERIVATION OF FOURIER TRANSFORMS TO MODEL SELF-FOCUSING

In one dimension, the paraxial wave equation, using retangular co-ordinates, is [3]

$$\frac{\partial E}{\partial z} = -\frac{i}{2k_0}\frac{\partial^2 E}{\partial x^2} \qquad \text{(Eq. C.1)}$$

The Fourier transform pair for the spatial domain field, $E(x,z)$, and the spatial frequency domain field, $\tilde{E}(\kappa,z)$, is [3]

$$\tilde{E}(\kappa,z) = \frac{1}{\sqrt{2\pi}}\int_{-\infty}^{\infty} E(x,z)\exp(-ix\kappa)dx \qquad \text{(Eq. C.2)}$$

$$E(x,z) = \frac{1}{\sqrt{2\pi}}\int_{-\infty}^{\infty} \tilde{E}(\kappa,z)\exp(ix\kappa)d\kappa \qquad \text{(Eq. C.3)}$$

where κ is the spatial frequency.

Taking the Fourier transform of both sides of the one dimensional paraxial equation, we get

$$\frac{d\tilde{E}(\kappa,z)}{dz} = \frac{i\kappa^2}{2k_0}\tilde{E}(\kappa,z) \qquad \text{(Eq. C.4)}$$

This is a simple differential equation, with solution

$$\tilde{E}(\kappa,z+\Delta z) = \tilde{E}(\kappa,z)\exp\left[\frac{i\kappa^2\Delta z}{2k_0}\right] \qquad \text{(Eq. C.5)}$$

where again Δz is the distance in the z direction the wave is propagated. To recover the spatial domain field at the exit plane, one simply takes the inverse Fourier transform of the result.

$$E(x, z+\Delta z) = \frac{1}{\sqrt{2\pi}} \int_{-\infty}^{\infty} \tilde{E}(\kappa, z) \exp\left[\frac{i\kappa^2 \Delta z}{2k_0} + ix\kappa\right] d\kappa \qquad \text{(Eq. 6)}$$

APPENDIX D

DERIVATION OF HANKEL TRANSFORM TO MODEL SELF-FOCUSING

A field is propagated through a given medium using the Hankel transform in the following manner. Let us start with the Hankel transform pair of a field, E(r,z), and its Hankel transform function, H(r,z), given as [50]

$$H(\rho,z)=2\pi\int_0^\infty E(r,z)J_0(2\pi\rho r)r\,dr \qquad \text{(Eq. D.1)}$$

$$E(r,z)=2\pi\int_0^\infty H(\rho,z)J_0(2\pi\rho r)\rho\,d\rho \qquad \text{(Eq. D.2)}$$

where r is the radial distance, ρ is the radial spatial Bessel frequency, and z is the longitudinal distance.

The Hankel transform itself was calculated using Siegman's method [48]. This allows one to use an FFT to find the Hankel transform in the following manner. For a given function, $f(r)$, the Hankel transform, $g(\rho)$, is given as [48]

$$g(\rho)=2\pi\int_0^\infty r f(r)J_0(2\pi\rho r)dr \qquad \text{(Eq. D.3)}$$

The change of variables is made [48]

$$r=r_0e^{\alpha x} \qquad \text{(Eq. D.4)}$$

$$\rho=\rho_0e^{\alpha y} \qquad \text{(Eq. D.5)}$$

converts the Hankel transform integral into a convolution integral, given as

$$g'(y) = \int_{-\infty}^{\infty} f'(x) j'(x+y) dx \qquad \text{(Eq. D.6)}$$

where

$$g'(y) = \rho g(\rho) \qquad \text{(Eq. D.7)}$$

$$f'(x) = r f(r) \qquad \text{(Eq. D.8)}$$

$$j'(x+y) = 2\pi\alpha r\rho J_0(2\pi r\rho) \qquad \text{(Eq. D.9)}$$

Since this is a convolution integral, the convolution was performed as a multiplication in Fourier space. For

$$F(\omega) = \frac{1}{\sqrt{2\pi}} \int_{-\infty}^{\infty} f'(x) \exp[-i\omega x] dx \qquad \text{(Eq. D.10)}$$

$$J(\omega) = \frac{1}{\sqrt{2\pi}} \int_{-\infty}^{\infty} j'(y) \exp[-i\omega y] dy \qquad \text{(Eq. D.11)}$$

Then, in Fourier space,

$$G(\omega) = F(\omega) J(\omega) \qquad \text{(Eq. D.12)}$$

The Hankel transform is recovered by using an inverse Fourier transform on the above result as [48]

$$g(y) = \frac{1}{\sqrt{2\pi}} \int_{-\infty}^{\infty} G(\omega) \exp[i\omega y] d\omega \qquad \text{(Eq. D.13)}$$

The the paraxial wave equation in cylindrical coordinates is given as [50]

$$\frac{\partial}{\partial z} E(r,z) = -\frac{i}{2k} \nabla_T^2 E(r,z) \qquad \text{(Eq. D.14)}$$

where k is the wave number and ∇_T^2 is the transverse Laplacian.

On taking the Hankel transform of both sides of Eq. (D.14), one gets [50]

$$\frac{\partial}{\partial z}H(\rho,z)=\frac{i2\pi^2\rho^2}{k}H(\rho,z) \qquad \text{(Eq. D.15)}$$

This is a simple differential equation, with solution

$$H(\rho,z+\Delta z)=H(\rho,z)\exp\left(\frac{i2\pi^2\rho^2}{k}\Delta z\right) \qquad \text{(Eq. D.16)}$$

where Δz is the longitudinal distance the field is propagated.

Taking the Hankel transform of Eq. (D.16) gives a formula for the paraxial propagation by a distance Δz of a cylindrically symmetric field, E(r,z), as

$$E(r,z+\Delta z)=2\pi\int_0^\infty H(\rho,z)\exp\left(\frac{i2\pi^2\rho^2}{k}\Delta z\right) \qquad \text{(Eq. D.17)}$$
$$\times J_0(2\pi\rho r)\rho\,d\rho$$

The following program is an example of a program the numerically models a beam propagating through a Kerr lens modelocked cavity. The beam is propagated using a Hankel transform version of the beam propagation method. Siegman's [48] method of using a FFT to perform a Hankel transform is used. The converging-diverging transformation of Szilkas and Siegman [47] is used as well. The cavity simulated is a ring cavity with two explicit curved mirrors, one nonlinear crystal, and one aperture. In this particular example, a 2 cm long nonlinear crystal with n_o = 1.75 and n_2 = 250 x 10^{-20} m^2/W is used. The aperture diameter in this example is 1.27 mm. The aperture is located 150 cm from mirror M_3.

An initially Gaussian beam is circulated through the cavity 100 times. The field is the square-root of the intensity and stored in a complex array E_wave. There are 70 nonlinear steps through the crystal. After propagation through the cavity 100 times, the program measures the per pass loss at the intracavity aperture, and writes it out, along with the current peak power tested. The program is written to actually perform 21 different power level tests, starting at 1 W and increasing in increments of 500 W to 10 kW.

Variables rs and roes are used to convert between scaled and unscaled beams. This is necessary when the diverging-converging transformation is used. Variables z0, z1, and z2 are used for diverging-converging transformations as well. This is scaled to match the mirror focus so that the transformation and mirror phase change can happen at one step.

The function BESSJ0 finds the Bessel function of a given input X. The subroutine FOUR1 takes a FFT of an array DATA of length NN. These programs are taken directly from Press, et al., Numerical Recipes [44].

Since in the Hankel space domain, all propagations are matrix multiplications, arrays primespace, d1space, d2space, gaincryspace, l1space, l2space, and l3space are used to store these matrix propagation values. Otherwise, the same complex numbers would have to be calculated for each pass through these regions. The primespace array propagates the

complex beam through the diverging-converging z' co-ordinate nearest to the mirrors in the focused portion of the cavity. Arrays d1space and d2space propagate the beam through the free-space region between the ends of the nonlinear crystal and the primed space. The array gaincryspace is a linear segment of the nonlinear crystal. In this example, it represents 1/70 of the distance through the 2 cm crystal. Arrays l1space, l2space, and l3space are free-space propagations through the longer portions of the ring cavity. Note that the aperture appears between l2space and l3space.

```
c     singcr.f single crystal ring cavity
c     this version places the nonlinear crystal in the focus
c     direction of propagation is counter-clockwise
c     last changes made April 5, 1992
c     all rights reserved
      implicit none
      integer steps,j,jj,crys_steps,N,NN,kk,jk,hops,jjj
      parameter (N=8192,NN=16384)
      real*8 d1,d2,cdzl,cdzg,P_init,P_fin,powersca-
le,loss,gain,delP
      real*8
z1,z2,focal_len,cav_len,dzp,dz,lambdanl,lambdang
      real*8 lambda, z,z0,w0,wz,r,del_r,pi,r_final,alpha
      real*8 omega,b,rprime,E1,E2,Ec,Croe,Hc,K1,K2,w0p,zf
      real*8 r0, roe, roe0, roe_final,del_z,exp_step,thrash
      real*8 r0s,roes,roe0s,l0,l1,l2,l3,scale,aperture
      real*8 P0,n2g,n0g,gammag,dead_len,delta_len,crys-
tal_leng
      real*8 n2l,n0l,gammal,crystal_lenl
      complex*16 J_nsf,J_sr,J_sf,J_nsr
      complex*16 l1space,l2space,primespace,d1space,d2space
      complex*16 gaincryspace,lenscryspace,l3space
      complex*16 i, k, phi,E_wave, Cord,temp
      dimension l1space(N),l2space(N),primespace(N),d1spa-
ce(N)
      dimension
d2space(N),gaincryspace(N),l3space(N),lenscryspace(N)
      dimension J_sr(NN),J_nsr(NN)
      dimension J_sf(NN),J_nsf(NN)
      dimension Cord(N),E_wave(NN)
```

```
      i = (0.0,1.0)
      pi = 4.0*atan(1.0)

      steps = 100
      crys_steps = 70
      hops = 21
      n0g = 1.75
      n2g = 3.0e-18
      n0l = 1.75
      n2l = 2.5e-18
      lambda = 830e-9
      lambdanl = lambda/n0l
      lambdang = lambda/n0g
      k = 2*pi/lambda
      gammag = 2.0*n2g*pi/lambda
      gammal = 2.0*n2l*pi/lambda
      focal_len = 0.05
      crystal_lenl = 0.020
      crystal_leng = 0.008
      cav_len = 0.111428571
      cdzl = crystal_lenl/crys_steps
      cdzg = crystal_leng/crys_steps
      write(*,*) 'cdzl=',cdzl
      write(*,*) 'cdzg=',cdzg
      dead_len = 0.004
      delta_len = 0.001
      l1 = 0.5
      l0 = 0.5
      l2 = 0.35
      l3 = l0 - l2
      d1 = dead_len + 3.0*delta_len
      d2 = dead_len - 3.0*delta_len
      delP = 500
      P0 = 1.0
      write(*,*) 'd1 =',d1
      write(*,*) 'crystal length =',crystal_leng
      write(*,*) 'n2 =',n2g
c     for this method, r is scaled by 2 pi
      w0 = 0.272e-3
      aperture = 0.635e-3
      scale = sqrt(2.0)/2/pi/w0
      r0s = 0.0001/scale
      roe0s = 0.0001*scale
      r_final = 30.0/scale
      write(*,*) 'rm (scaled) = ', r_final/2/pi
      alpha = ( log ( r_final / r0s ) ) / ( N - 1 )
      write(*,*) 'alpha = ',alpha
      write(*,*) 'roe0s = ',roe0s
      z0 = 0.004 + dead_len + (focal_len - cav_len/2.0)
      z1 = z0
      z2 = focal_len
      write(*,*) 'z1=',z1
      write(*,*) 'z2=',z2
```

```
      dzp = z0*(z2-z1)/z2
      write(*,*) 'dzp=',dzp
c     scale nonlinear factor gamma
      gammal = gammal*z1*z1/z2/z2
      call init_J(NN,J_sf,r0s,roe0s,alpha)
      call init_J(NN,J_sr,roe0s,r0s,alpha)
c     scale r axis
c     scale roe as well
      r0 = r0s*z1/z2
      roe0 = roe0s*z2/z1
      call init_J(NN,J_nsf,r0,roe0,alpha)
      call init_J(NN,J_nsr,roe0,r0,alpha)
      call initcoord(N,r0,alpha,lambda,Cord,z1)
      call init_space(l1space,N,roe0s,alpha,l1,lambda)
      call init_space(l2space,N,roe0s,alpha,l2,lambda)
      call init_space(l3space,N,roe0s,alpha,l3,lambda)
      call init_space(primespace,N,roe0,alpha,dzp,lambda)
      call init_space(d1space,N,roe0,alpha,d1,lambda)
      call init_space(d2space,N,roe0,alpha,d2,lambda)
      call init_space(gaincryspace,N,roe0,alpha,cdzg,lamb-
dang)

open(UNIT=13,FILE='singcr.35cm+3d1CdS+',STATUS='UNKNOWN')
      rewind(13)
      do 1313 jjj=1,hops
c     initialize waveform
      call init_wave(N,NN,alpha,r0s,E_wave,z1,z2,P0,w0)
      powerscale = z1/z2
      call powercalc(E_wave,N,P_init,r0s,alpha,powerscale)
      write(*,*) 'initial power =',P_init
      do 999 kk=1,steps
        write(*,*) 'steps',kk
        call prop(E_wave,J_sf,N,NN,r0s,roe0s,alpha,l1spa-
ce,J_sr)
        call
prop(E_wave,J_nsf,N,NN,r0,roe0,alpha,primespace,J_nsr)
        call coord(N,E_wave,Cord)
        call prop(E_wave,J_nsf,N,NN,r0,roe0,alpha,d1spa-
ce,J_nsr)
        do 62 jj = 1,crys_steps
         call prop(E_wave,J_nsf,N,NN,r0,roe0,alpha,gaincry-
space,J_nsr)
         call nonlin(E_wave,N,gammag,cdzg)
62      continue
        call prop(E_wave,J_nsf,N,NN,r0,roe0,alpha,d2spa-
ce,J_nsr)
        call coord(N,E_wave,Cord)
        call prop(E_wave,J_nsf,N,NN,r0,roe0,alpha,prime-
space,J_nsr)
        call
prop(E_wave,J_sf,N,NN,r0s,roe0s,alpha,l3space,J_sr)
        do 63 j=1,N
           r=r0s*exp(alpha*(j-1))
```

```
            rprime = r/2/pi
            if (rprime .GT. aperture ) then
              E_wave(j) = 0.0
            end if
63        continue
          call powercalc(E_wave,N,P_fin,r0s,alpha,powerscale)
          gain = sqrt(P_init/P_fin)
          write(*,*) 'gain =',gain
          loss = 1.0 - P_fin/P_init
          write(*,*) 'loss=',loss
          do 66  j=1,N
66          E_wave(j) = gain*E_wave(j)
          call prop(E_wave,J_sf,N,NN,r0s,roe0s,alpha,l2spa-
ce,J_sr)
999     continue
        write(13,*) P0/1000.,loss
        P0 = P0 + delP
1313    continue
c       output follows
        open(UNIT=11,FILE='singcre',STATUS='UNKNOWN')
        rewind(11)
        do 15 j=N/4,N,8
          r = r0s*exp(alpha*(j-1))
          rprime = r/2/pi
          temp = E_wave(j)
          temp = z1/z2*temp
          write(11,*) rprime,abs(temp)**2
15      continue
626     write(*,*) 'end of process'
        close(10)
        close(11)
        close(13)
        end
```

The subroutine hankel performs the Hankel transform on a complex array E_wave with stored Bessel coefficients in J_coeff, of length N and 2*N = NN for a starting values of r0 and roe0 and for a giving scaling factor of alpha. The method is based upon that of Siegman [48] and uses an FFT to calculate the Hankel transform for an exponential scale.

```
      subroutine hankel(E_wave,J_coeff,N,NN,r0,roe0,alpha)
      implicit NONE
      integer N,NN,j,isign
      real*8 pi,r0,roe0,alpha,omega,exp_step,r,thrash
      real*8 roe
      complex*16 E_wave, i, Ec,Croe
      complex*16 J_coeff
      dimension E_wave(*),J_coeff(*)
      i = (0.0,1.0)
      pi = 4.0*atan(1.0)
c     Ec is used for the correction step
      Ec = E_wave(1)
      do 1 j=1,N
        omega = alpha*(j-1)
        exp_step = exp(omega)
        r = r0*exp(alpha*(j-1))
        E_wave(j) = r*E_wave(j)
1     continue
      do 2 j=N+1,NN
        E_wave(j) = 0.0
2     continue
c     FFT(fm)
      isign = 1
      call four1(E_wave,NN,isign)
c     gm = FFT(FFT(fm) * FFT*(jm))
      do 3 j = 1,NN
        E_wave(j) = E_wave(j)*J_coeff(j)
3     continue
      isign = 1
      call four1(E_wave,NN,isign)
      do 40 j=1,N
        omega = alpha*(j-1)
        roe = roe0*exp(omega)
        Croe = Ec*0.5*r0*r0*(1-0.125*roe*roe*r0*r0)
        E_wave(j) = E_wave(j)/roe/NN + Croe
40    continue
      do 5 j = N+1,NN
        E_wave(j) = 0.0
5     continue
      return
      end
```

The subroutine init_wave initializes the beam distribution. Notice that the distribution is assumed to be TEM_{00} with a given beam waist, w_o, of w0 and power of P0. The variables alpha and r0 are required for the exponential distributed sample points used in the FFT method to find the Hankel transform. Variables z1 and z2 are used to scale the beam from the diverging-converging method.

```
      subroutine init_wave(N,NN,alpha,r0,E_wave,z1,z2,P0,w0)
      implicit none
      integer j,N,NN
      real*8 P0,omega,pi,E0,alpha,r0,z1,z2,w0,exp_step
      real*8 r,rprime
      complex*16 E_wave, temp
      dimension E_wave(*)
      pi = 4.0*atan(1.0)
      open(UNIT=10,FILE='singcri',STATUS='UNKNOWN')
      rewind(10)
      E0 = sqrt(P0*4.0/pi/w0/w0)*z2/z1
      write(*,*) 'E0 = ',E0
      write(*,*) 'z2/z1= ',z2/z1
      do 1 j=1,N
        omega = alpha*(j-1)
        exp_step = exp(omega)
        r = r0*exp_step
        rprime = r/2/pi
        E_wave(j) = E0*exp(-rprime*rprime/w0/w0)
1     continue
      do 2 j=N+1,NN
        E_wave(j) = 0.0
2     continue
      do 3 j=N/4,N,8
        omega = alpha*(j-1)
        exp_step = exp(omega)
        r = r0*exp_step
        rprime = r/2/pi
        temp = E_wave(j)
        temp = z1/z2*temp
        write(10,*) rprime,abs(temp)**2
3     continue
      return
      end
```

The subroutine init_J is used to store the Bessel coefficients for the Hankel transform.

```
      subroutine init_J(NN,J_coeff,r0,roe0,alpha)
      implicit none
      integer j,NN,isign
      real*8 r0,roe0,alpha,r,thrash,exp_step,bessj0
      complex*16 J_coeff
      dimension J_coeff(*)
      do 1 j=1,NN
        exp_step = exp(alpha*(j-1))
        r = r0*exp_step
        thrash = r0*roe0*exp_step
        J_coeff(j) = alpha*thrash*bessj0(thrash)
1     continue
c     FTT*(jm)
      isign = -1
      call four1(J_coeff,NN,isign)
      return
      end
      subroutine coord(N,E_wave,Cord)
      implicit none
      integer N,j
      complex*16 E_wave,Cord
      dimension E_wave(*),Cord(*)
      do 1 j=1,N
         E_wave(j) = E_wave(j)*Cord(j)
1     continue
      return
      end
```

The subroutine initcoord stores the exponentially distributed radial sample points required for the FFT method of calculation of the Hankel transform.

```
      subroutine initcoord(N,r0,alpha,lambda,Cord,z1)
      implicit none
      integer N,j
      real*8 pi,r0,alpha,lambda,z1,r,rprime
      complex*16 i,phi,Cord
      dimension Cord(*)
      i = (0.0,1.0)
      pi = 4.0*atan(1.0)
      do 10 j=1,N
        r = r0*exp(alpha*(j-1))
        rprime = r/2/pi
        phi = i*pi/z1/lambda*rprime*rprime
        Cord(j) = cdexp(phi)
10    continue
      return
      end
```

The subroutine init_space stores values for Hankel domain beam propagation by matrix multiplication.

```
      subroutine init_space(space,N,roe0,alpha,dz,lambda)
      implicit none
      integer j,N
      real*8 alpha,roe0,roe,lambda,pi,dz
      complex*16 i,phi,space
      dimension space(*)
      i = (0.0,1.0)
      pi = 4.0*atan(1.0)
      do 4 j = 1,N
         roe = roe0*exp(alpha*(j-1))
         phi = i*dz*pi*lambda*roe*roe
         space(j) = cdexp(phi)
4     continue
      return
      end
```

The subroutine nonlin performs the nonlinear phase correction on the complex beam.

```
      subroutine nonlin(E,N,gamma,cdz)
      implicit none
      integer j,N
      real*8 gamma, cdz
      complex*16 E, i, phi
      dimension E(*)
      i = (0.0,1.0)
      do 1 j=1,N
        phi = -i*gamma*cdz*E(j)*conjg(E(j))
        E(j) = E(j)*exp(phi)
1     continue
      return
      end
```

The subroutine powercalc calculates the power lost per pass at the aperture.

```
      subroutine powercalc(E,N,power,r0,alpha,scale)
      implicit none
      integer j,N
      real*8 power,r0,alpha,r,dr,pi,scale,rp,drp
      complex*16 E,temp
      dimension E(*)
      pi = 4.0*atan(1.0)
      power = 0.0
         r = r0
         rp = r/2/pi
         dr = r0*exp(alpha) - r
         drp = dr/2/pi
         temp = E(1)*scale
         power = power + temp*conjg(temp)*rp*drp
      do 1 j=2,N
         r = r0*exp(alpha*(j-1))
         rp = r/2/pi
         dr = (r0*exp(alpha*(j)) - r0*exp(alpha*(j-2)))/2.0
         drp = dr/2/pi
         temp = E(j)*scale
         power = power + temp*conjg(temp)*rp*drp
1     continue
      power = power*pi
      return
      end
```

The subroutine prop performs the matrix multiplication in the Hankel domain for linear complex beam propagation.

```
      subroutine prop(E,Jf,N,NN,r0,roe0,alpha,space,Jr)
      implicit none
      integer j,N,NN
      real*8 r0,roe0,alpha
      complex*16 E,Jf,Jr,space
      dimension E(*),Jf(*),Jr(*),space(*)
      call hankel(E,Jf,N,NN,r0,roe0,alpha)
      do 4 j = 1,N
         E(j) = E(j)*space(j)
4     continue
      call hankel(E,Jr,N,NN,roe0,r0,alpha)
      return
      end
```

APPENDIX E

CORRECTION FOR GROUP VELOCITY DISPERSION USING PRISM PAIR

Correction for Group Velocity Dispersion (GVD) using a prism pair is one method of reducing the effects of first order dispersion in the fs Ti:sapphire laser. The method used is based upon the earlier work of Fork, et al. [21]. Their work showed how a prism pair, made of a material with positive dispersion, can be arranged such that the cavity has negative dispersion.

Fork, et al., give the dispersion of the cavity, $d^2P/d\lambda^2$, as

$$\frac{d^2P}{d\lambda^2} = 4l\left\{\left[\frac{d^2n}{d\lambda^2} + \left(2n - \frac{1}{n^3}\right)\left(\frac{dn}{d\lambda}\right)^2\right]\sin\beta - 2\left(\frac{dn}{d\lambda}\right)^2\cos\beta\right\} \qquad \text{(Eq. E.1)}$$

where

l is the distance between the apex of the prisms,

n is the index of refraction of the prisms,

λ is the free space wavelength of interest, and

β is the propagation angle of a ray with respect to a reference line drawn between the apex of the two prisms.

The angle β is assumed to be small such that

$$l\sin\beta \cong 2\text{mm} \qquad \text{(Eq. E.2)}$$

$$\cos\beta \cong 1 \qquad \text{(Eq. E.3)}$$

Such a small path through the prisms is necessary to minimize the thermal effects of the prisms and to minimize the distance l. With the assumptions above, Eq. (E.1) simplifies to:

$$\frac{d^2P}{d\lambda^2} = 0.008\left[\frac{d^2n}{d\lambda^2} + \left(2n - \frac{1}{n^3}\right)\left(\frac{dn}{d\lambda}\right)^2\right] - 0.004\,l\left(\frac{dn}{d\lambda}\right)^2 \qquad \text{(Eq. E.4)}$$

For example, for prisms made of SF10 glass, at a wavelength of 800 nm, this glass has [2]

$$n = 1.71125$$

$$dn/d\lambda = -0.04958\,\mu\text{m}^{-1}$$

$$d^2n/d\lambda^2 = 0.1755\,\mu\text{m}^{-2}$$

Then Eq. (E.4) gives

$$d^2P_{SF10}/d\lambda^2 = 8\text{mm}\{0.1755\,\mu\text{m}^{-2} + [2(1.77125) - 1/(1.77125)^3] \times (-0.04958\,\mu\text{m}^{-1})^2\} - 8l_{SF10}(-0.04958\,\mu\text{m}^{-1})^2$$

$$d^2P_{SF10}/d\lambda^2 = 1.467 - l_{SF10}(1.967 \times 10^{-2})\text{mm}\cdot\mu\text{m}^{-2} \qquad \text{(Eq. E.5)}$$

Distance l required for correction of GVD passing through a given length of material in the cavity is calcu-

lated dividing dispersion in the cavity, $d^2P/d\lambda^2$, by the product of the second order dispersion of the material, $d^2n_M/d\lambda^2$, and the thickness of the material, t. Then,

$$-d^2n_M/d\lambda^2 t = d^2P/d\lambda^2 \qquad \text{(Eq. E.6)}$$

which, for SF10 reduces to,

$$-d^2n_M/d\lambda^2 t = 1.467 - l_{SF10}(1.967 x 10^{-2})\text{mm}\cdot\mu\text{m}^{-2} \qquad \text{(Eq. E.7)}$$

Then, for $d^2n_M/d\lambda^2$ given in μm^{-2} and t and l in mm, the distance between prism apex (using SF10 glass) is

$$l_{SF10} = 74.62 + 50.87 d^2n_M/d\lambda^2 t \qquad \text{(Eq. E.8)}$$

For example, for 6.5 mm sample of ZnS, with $d^2n/d\lambda^2 = 0.7\mu m^{-2}$, we find that l_{SF10} is about 306 mm, or 12 inches.

APPENDIX F

CALCULATION OF NONLINEAR INDEX OF REFRACTION

The numerical values of the nonlinear index of refraction for a materials presented in this report were obtained either through references or by calculations based on the method of Boling, et al. [56]. In the case of ZnS, CdS, quartz and Ti:sapphire, the work of Adair, et al. [53] was used as a reference. In this reference, n_2 was measured at 1.06 μm. For CZ, ZnSe, and SF11 glass, the values were calculated. In the case of calculations of n_2, the method of Boling, et al., gives an estimate of n_2 at 486 nm. Note that Boling, et al., state that the variations in measured results and calculations often give answers that vary more than a factor of two. Thus the values for n_2 presented in this report are to be used to estimate the relative strength of the nonlinearity of the materials only.

One of the more confusing problems encountered is that of the units for n_2. Note that the units will depend on first exactly which n_2 is being referred to as well as which system of units (MKS or cgs) is being used.

The relation between the linear and the nonlinear index of refraction can be presented as

$$n = n_0 + n_2 I \qquad \text{(Eq. F.1)}$$

$$= n_0 + n'_2 \langle E^2 \rangle \qquad \text{(Eq. F.2)}$$

$$= n_0 + \frac{n'_2}{2} |E^2| \qquad \text{(Eq. F.3)}$$

Using the relation between the intensity, I, and optical field, E, as [36]

$$I = \frac{1}{\eta} \langle E^2 \rangle \qquad \text{(Eq. F.4)}$$

$$= \frac{1}{2\eta} |E^2| \qquad \text{(Eq. F.5)}$$

where the characteristic impedance of a dielectric, η, is related to the permittivity of a medium, ϵ, the permittivity of free space, ϵ_0, the permeability of free space, μ_0, and the index of refraction of the medium, n, as [57]

$$\eta = \sqrt{\frac{\mu_0}{\epsilon}} \qquad \text{(Eq. F.6)}$$

$$= \frac{1}{n}\sqrt{\frac{\mu_0}{\epsilon_0}} \qquad \text{(Eq. F.7)}$$

Note that, in MKS units, η = 377 Ω. The relation between the two variations of n_2 (n_2 and n'_2) is given as

$$n_2 = n'_2 \frac{377\,\Omega}{n} \qquad \text{(Eq. F.8)}$$

The units for n'_2 presented in many texts is esu. The conversion to n'_2 in MKS units is given as [58]

$$n'_2(\text{MKS}) = \frac{1}{9} \times 10^{-8} n'_2(\text{esu}) \qquad \text{(Eq. F.9)}$$

Thus the conversion from n'_2 in esu presented in most texts to n_2 in MKS units of m^2/W is

$$n_2(\mathrm{MKS}) = \frac{4.19 \times 10^{-8}}{n} n'_2(\mathrm{esu}) \qquad \text{(Eq. F.10)}$$

The following program is used estimate the nonlinear index of refraction, n_2, for ZnS, based on the method of Boling, et al. [56]. The result is in units of 10^{-13} esu. The linear index of refraction is estimated using the dispersion formula given by Weber [59].

```
      implicit none
      integer i,j,k,steps
      real*8 l,n,n2,nsq,power,c
      real*8 Atemp,A, nn,disp,gvd
      real*8 lf,ld,lc,nf,nd,nc,vd, numer, denom
      steps = 10
      c = 299.792458e6
c     wavelength dimensions must be in microns
c     program reads dispersion formula coefficients from
file 'ior.coef'
c     and writes index of refraction result to file
'ior.data'
      lf = 4861
      ld = 5875
      lc = 6563
      l = lf
      nsq = 5.131 + 1.275e7/(l*l-0.732e7)
      nf = sqrt(nsq)
    write(*,*) 'nf=',nf
      l = ld
      nsq = 5.131 + 1.275e7/(l*l-0.732e7)
      nd = sqrt(nsq)
    write(*,*) 'nd=',nd
      l = lc
      nsq = 5.131 + 1.275e7/(l*l-0.732e7)
      nc = sqrt(nsq)
    write(*,*) 'nc=',nc
      vd = (nd-1)/(nf-nc)
      numer = 68.0*(nd-1)*((nd*nd+2)**2)
      denom = 1.517 + vd*(nd*nd+2)*(nd+1)/6/nd
      denom = vd*sqrt(denom)
      n2 = numer/denom
      write(*,*) 'n2 = ',n2
      write(*,*) 'end of process'
      end
```

APPENDIX G

CALCULATION OF ASTIGMATISM CORRECTION

Calculation of the proper angle to correct for astigmatism of a element placed at the Brewster angle near the focus of a beam was based upon the method developed by Kogelnik, et al. [60]. The half angle θ for proper astigmatic correction is given as

$$Nt = R \sin\theta \tan\theta \qquad \text{(Eq. G.1)}$$

where t is the thickness of the Brewster plate, R is the radius of the mirrors, and N is given as

$$N = \frac{n^2 - 1}{n^4}\sqrt{n^2 + 1} \qquad \text{(Eq. G.2)}$$

For example, to correct for the astigmatism in a 6.3 mm thick piece of SF11 glass (n = 1.77), we get for N

$$N = \frac{1.77^2 - 1}{1.77^4}\sqrt{1.77^2 + 1}$$

$$= 0.442$$

For R = 10 cm,

$$\sin\theta \tan\theta = \frac{Nt}{R}$$

$$= 0.0278$$

for which 2θ = 19 degrees is a valid solution.

The following fortan program calculates N for astigmatism correction

```
c   capn.f calculate N for astigmatism
    implicit none
    integer i
    real n, capn, t, theta, pi, error, del, R
    real RHS,LHS

    pi = 4.0*atan(1.0)
    del = 0.001
    write(*,*) 'enter index of refraction'
    read(*,*) n
    capn = (n*n-1)*sqrt(n*n+1)/n/n/n/n
    write(*,*) 'N = ',capn
    write(*,*) 'enter thickness of material (cm)'
    read(*,*) t
    R = 10
    RHS = capn*t/R
    write(*,*) 'Nt/R =',RHS
    theta = pi/180
    do i=1,20
      LHS=sin(theta)*tan(theta)
      write(*,*) theta*180/pi,LHS
      theta = theta+1.0*pi/180
    end do
    end
```

APPENDIX H

FIGURES

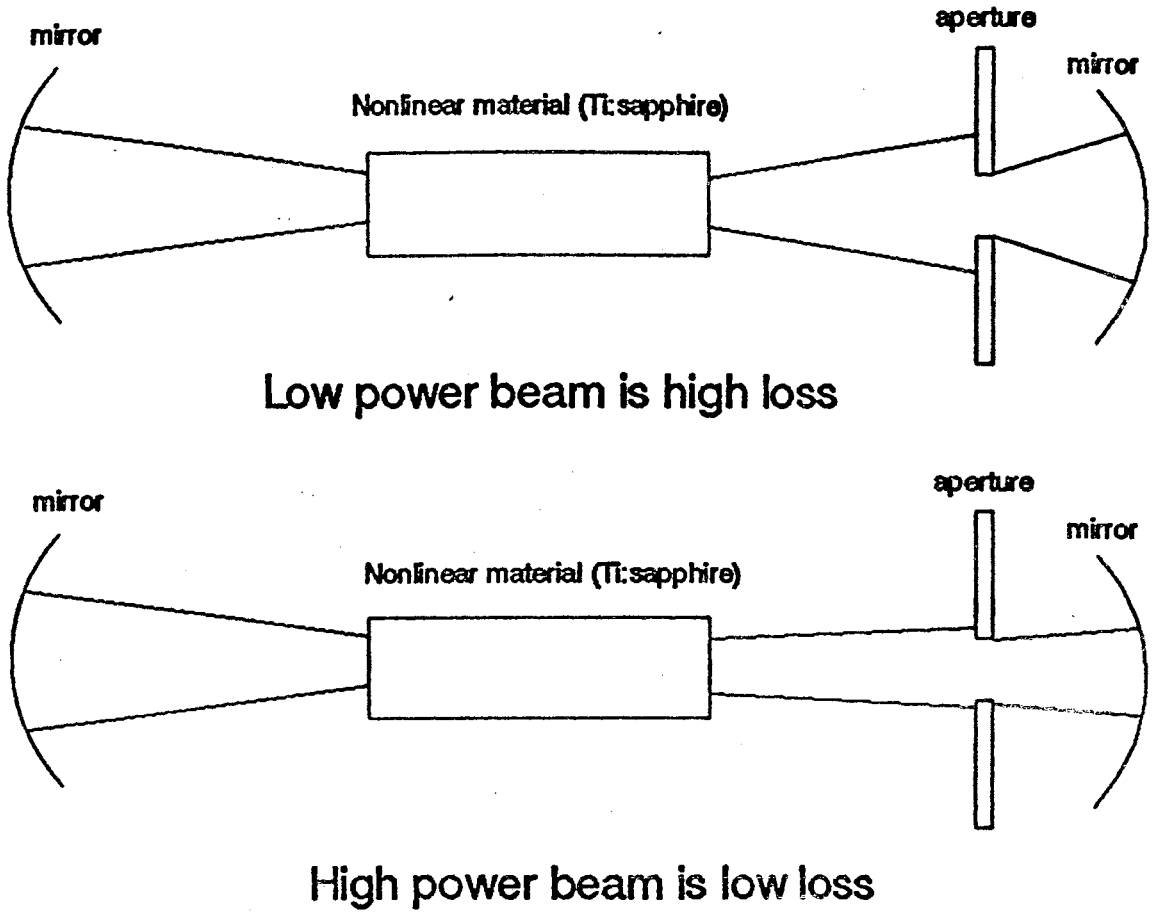

Figure 1. Beam profiles in simplified KLM laser cavity. Low power beam suffers larger losses due to aperture losses. Higher power beam has less loss at aperture due to self-focusing.

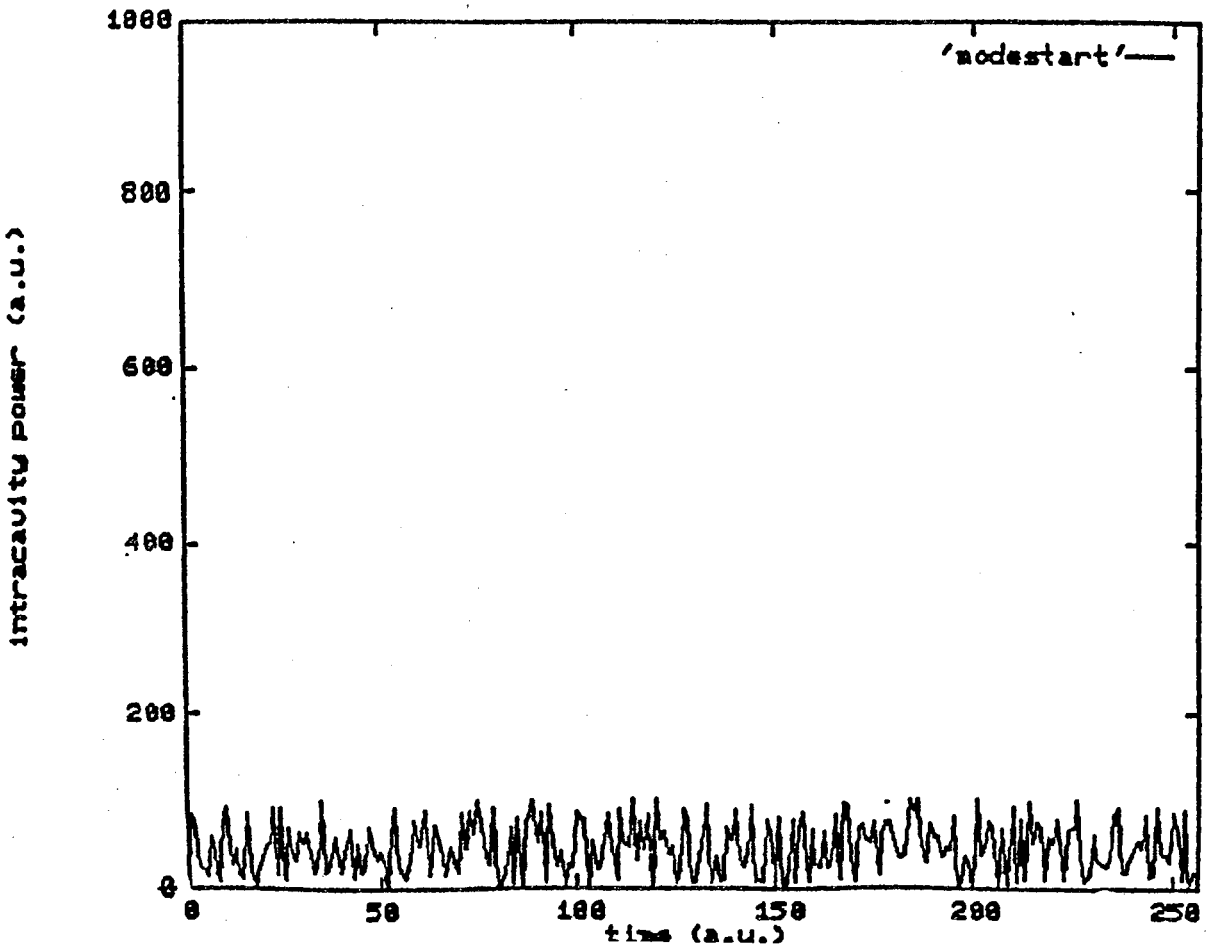

Figure 2. Simulation results for linear loss model of modelocking. Shown is the temporal envelope of intracavity beam in a cavity with many longitudinal modes (10^4 to 10^5).

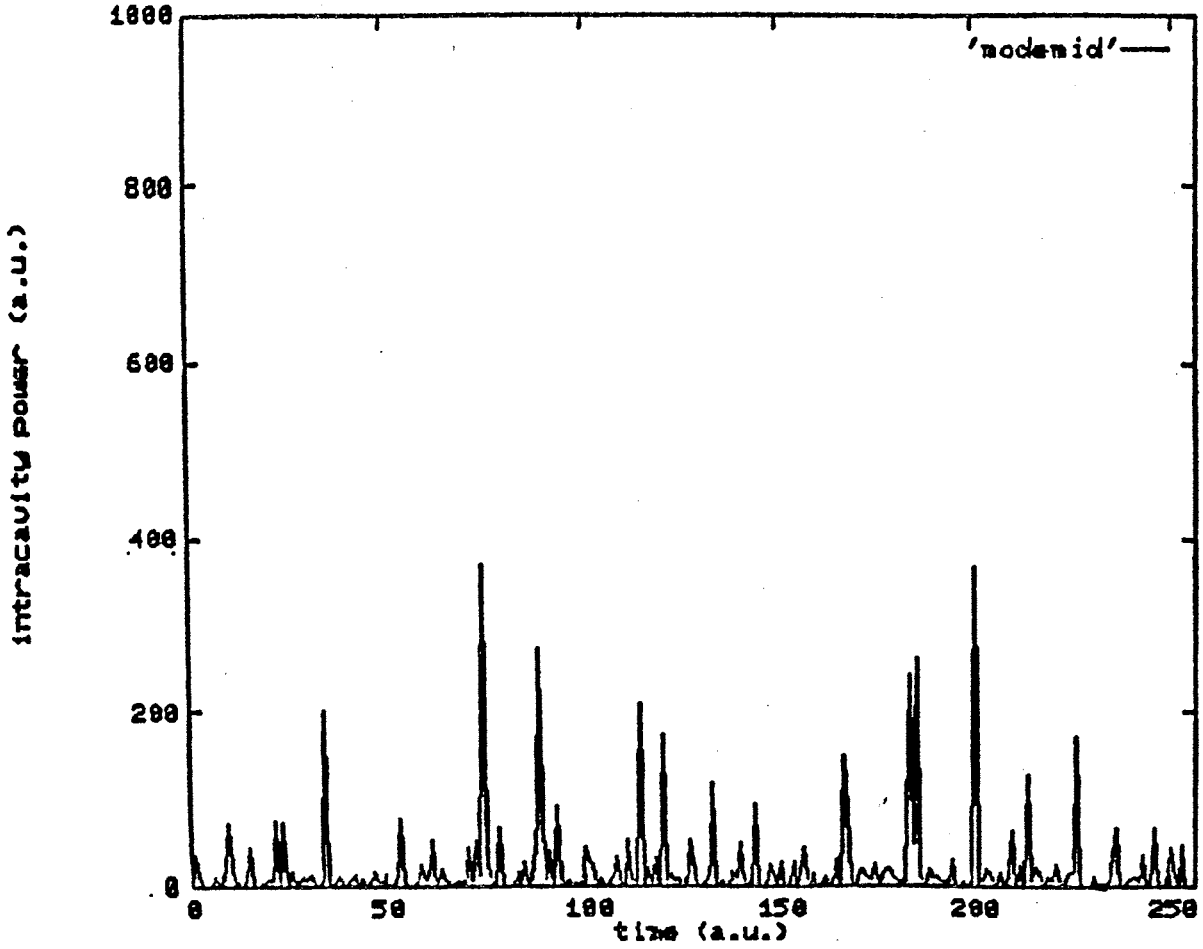

Figure 3. Same cavity as shown in Figure 2 after 2,000 round trips through the cavity using linear loss model of modelocking.

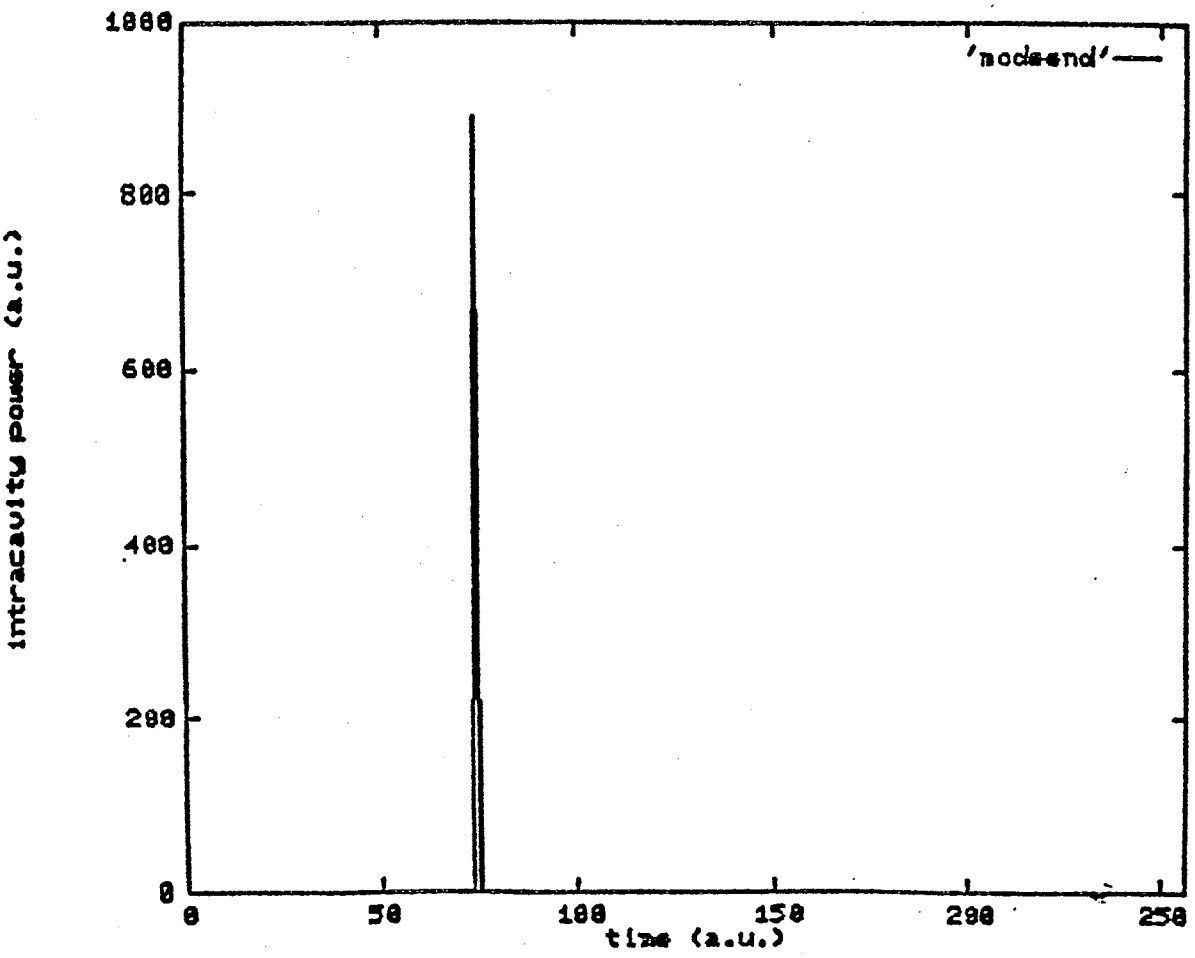

Figure 4. Same cavity as shown in Figure 2 after 5,000 round trips using linear loss model of modelocking. Laser is 'mode-locked'.

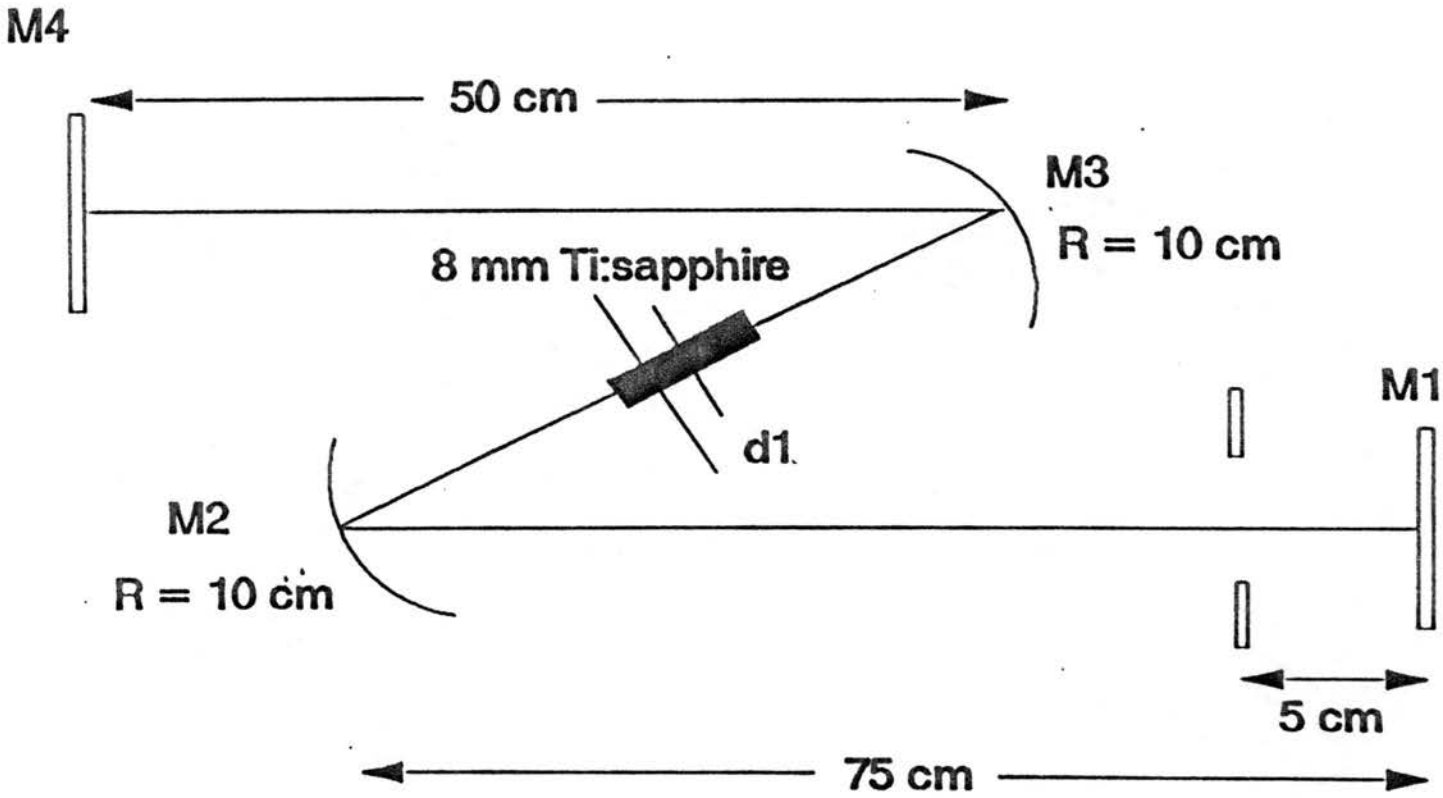

Figure 5. Schematic of cavity simulated in thin-lens approximation of self-modelocking in a KLM laser.

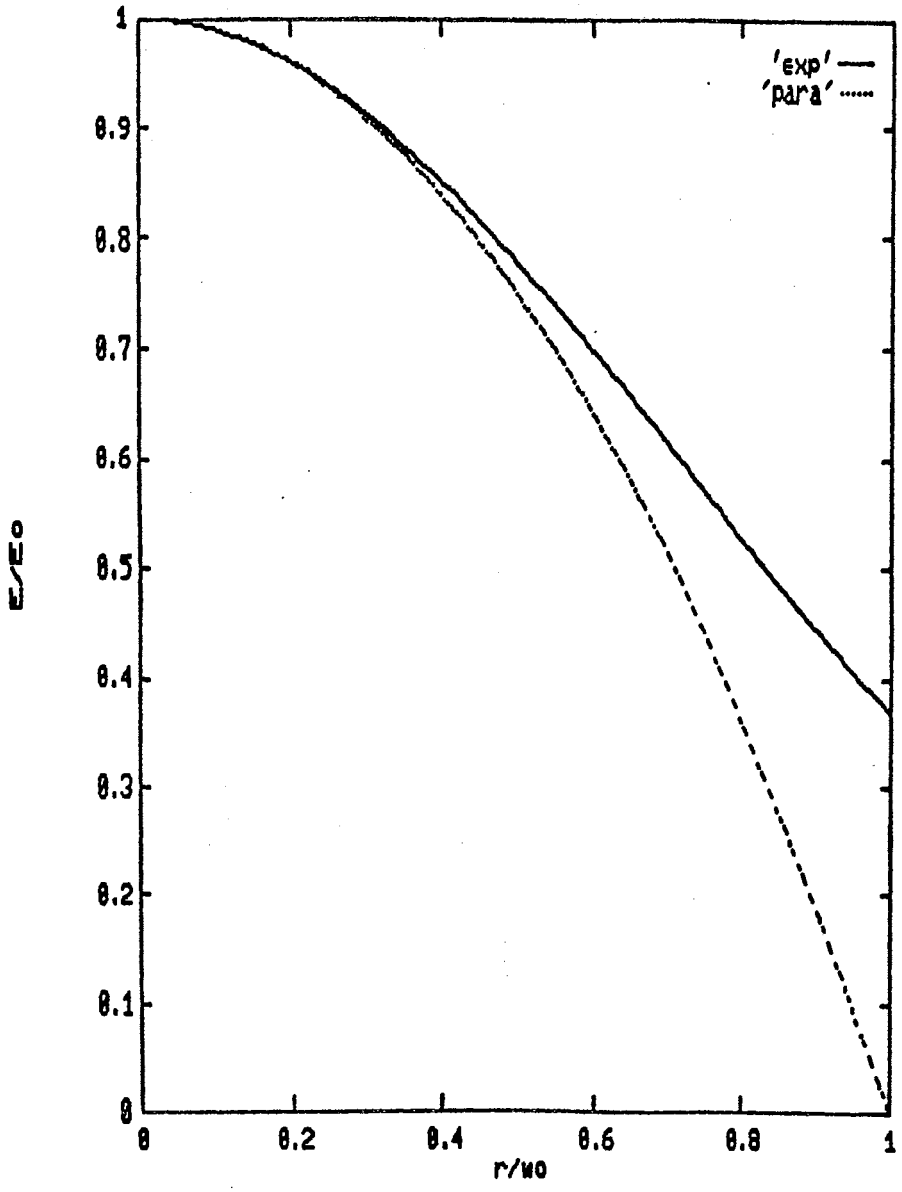

Figure 6. Comparison of parabolic fit to exponential function in parabolic GRIN lens approximation of self-focusing. The curve 'exp' is the exponential curve function while the curve 'para' is the parabolic approximation.

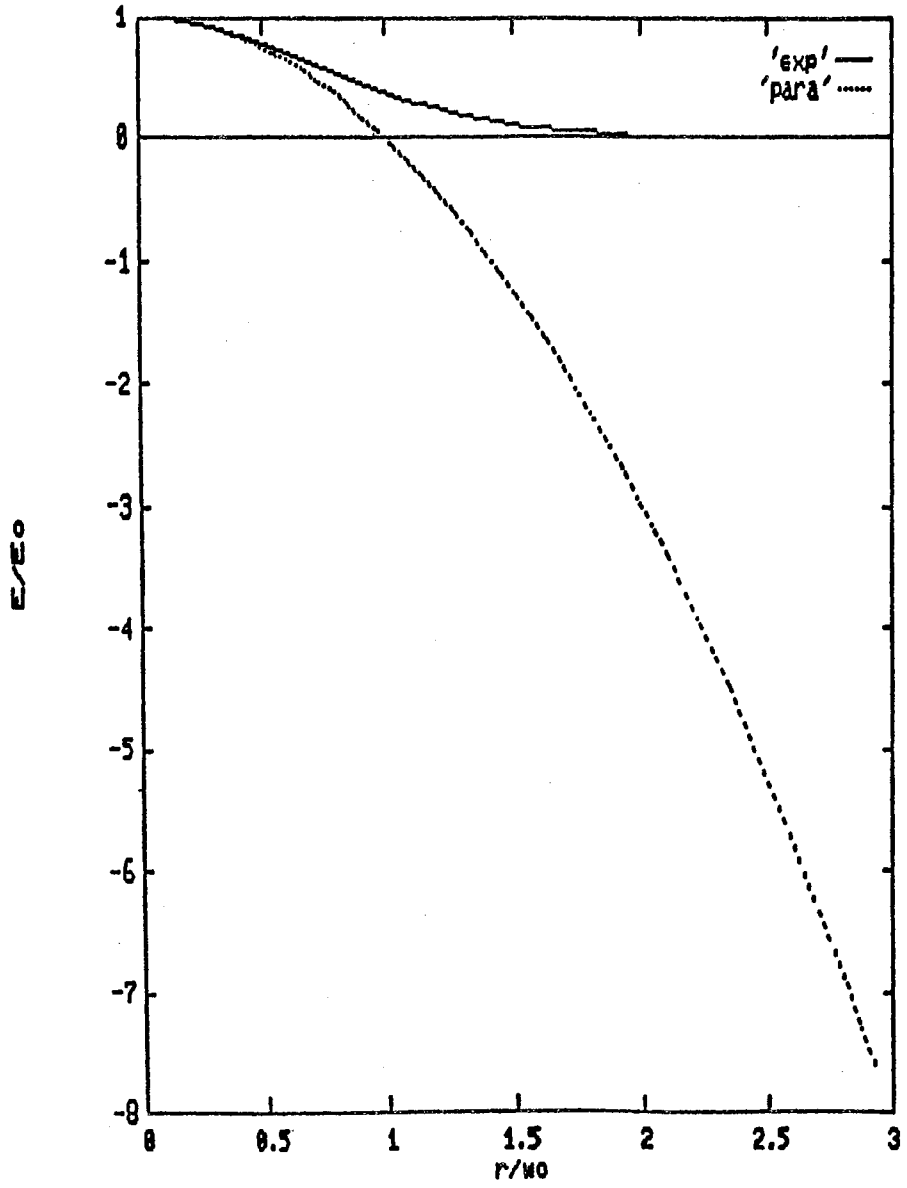

Figure 7. Comparison of parabolic fit to exponential function as is shown in Figure 6 with normalized radius extended to r = 3 w_o.

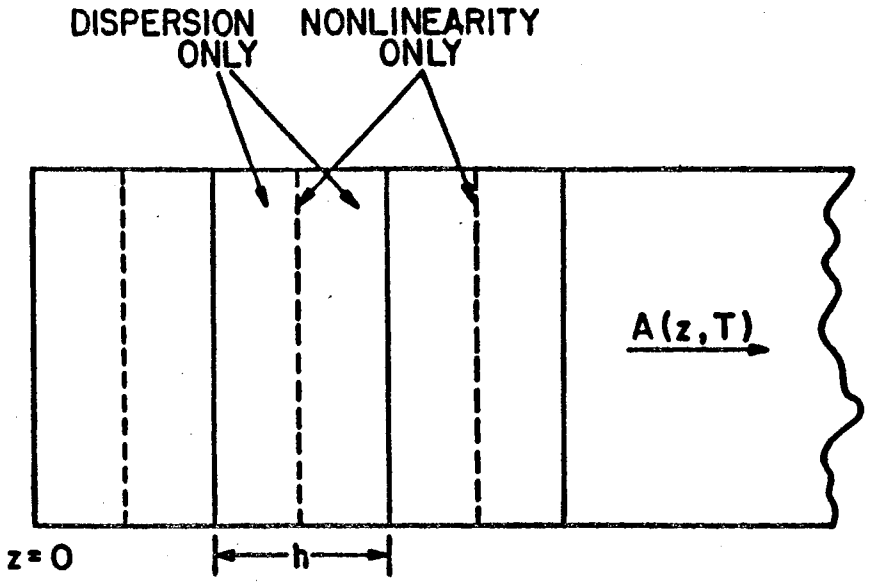

Figure 8. Schematic of split-step beam propagation method used for numerical simulations. The nonlinear element is divided up into a large number of segments of length h. Within each segment, the effect of self-focusing is included as a phase correction. (After Ref. [33]).

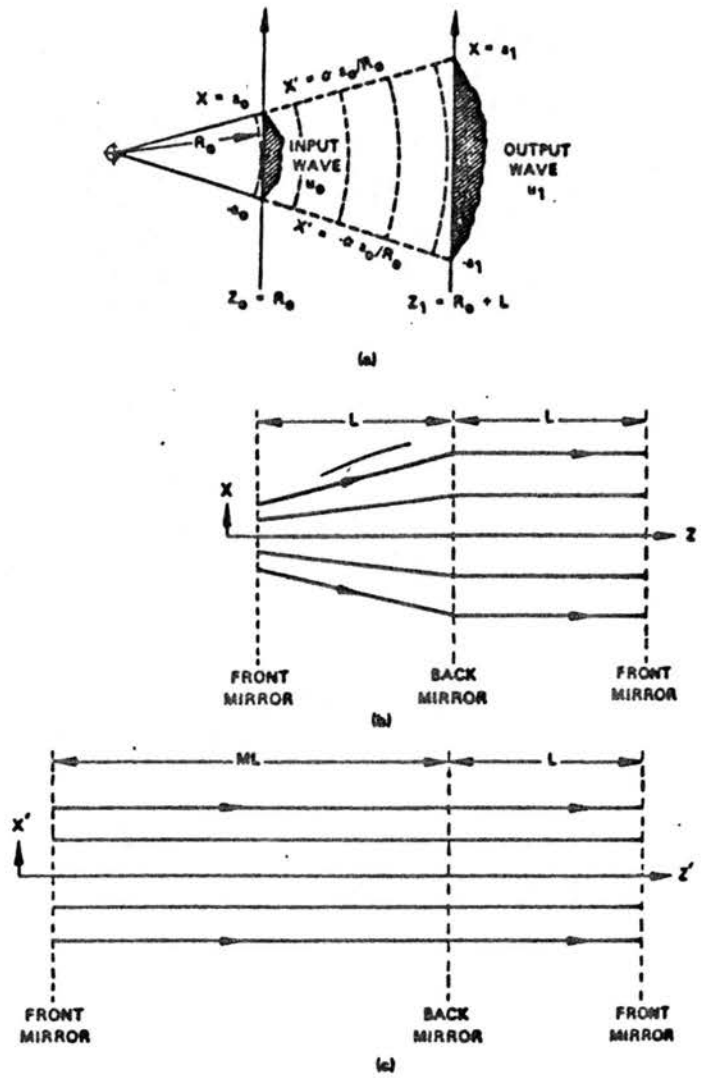

Figure 9. Schematic of diverging quasi-spherical wave optical beam. Expanded coordinate system allows more efficient gird sampling of tightly focused beam. (After Ref. [47]).

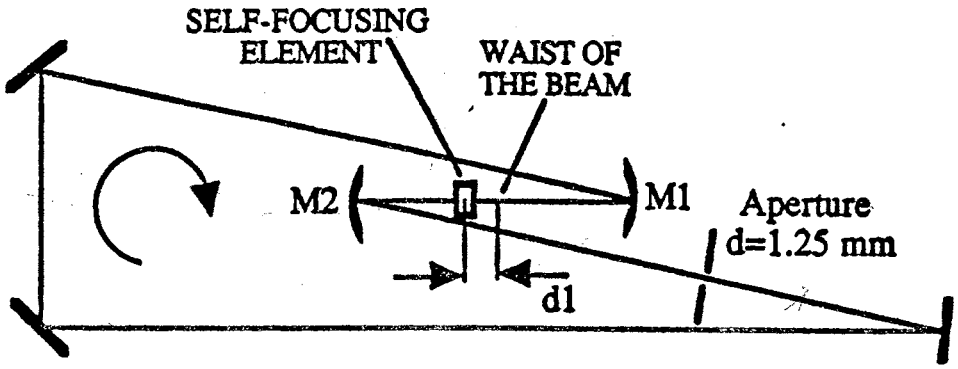

Figure 10. Ring KLM laser with highly nonlinear element used in Hankel transforms beam propagation simulations. Curved arrow shows direction of beam propagation.

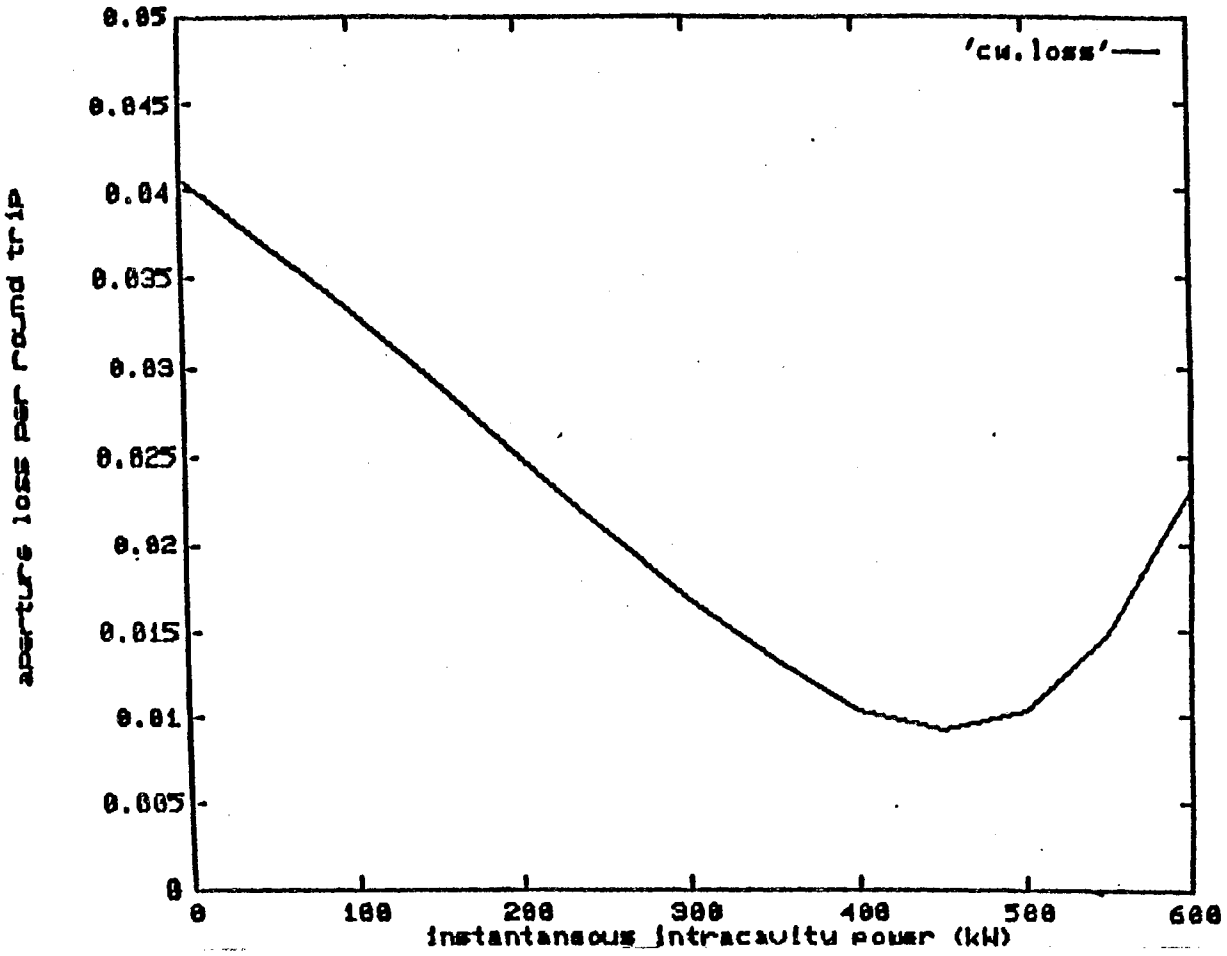

Figure 11. Aperture loss per round trip vs. intracavity power in linear cavity Ti:sapphire KLM laser using Hankel transform beam propagation method.

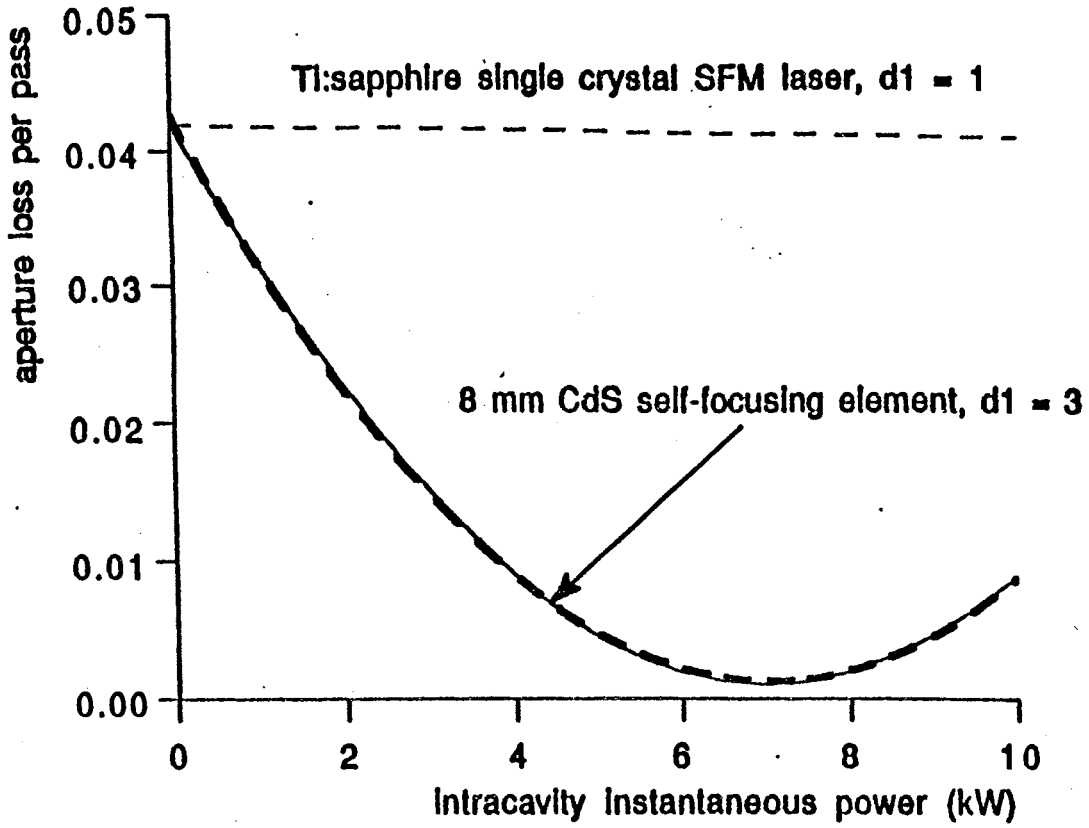

Figure 12. Aperture loss per round trip vs. intracavity power in ring cavity KLM simulations using Hankel transform beam propagation method.

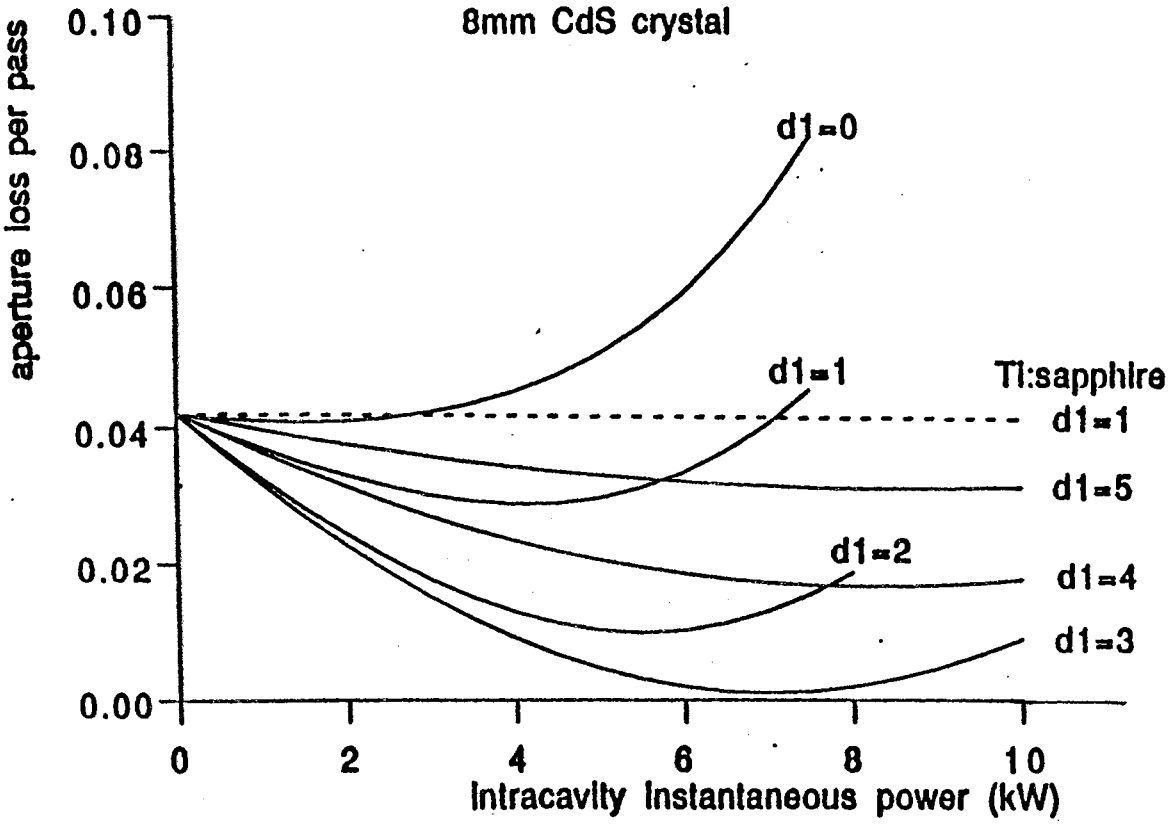

Figure 13. Aperture loss per round trip vs. intracavity power for various crystal positions for same laser shown in Figure 10 using Hankel transform beam propagation method.

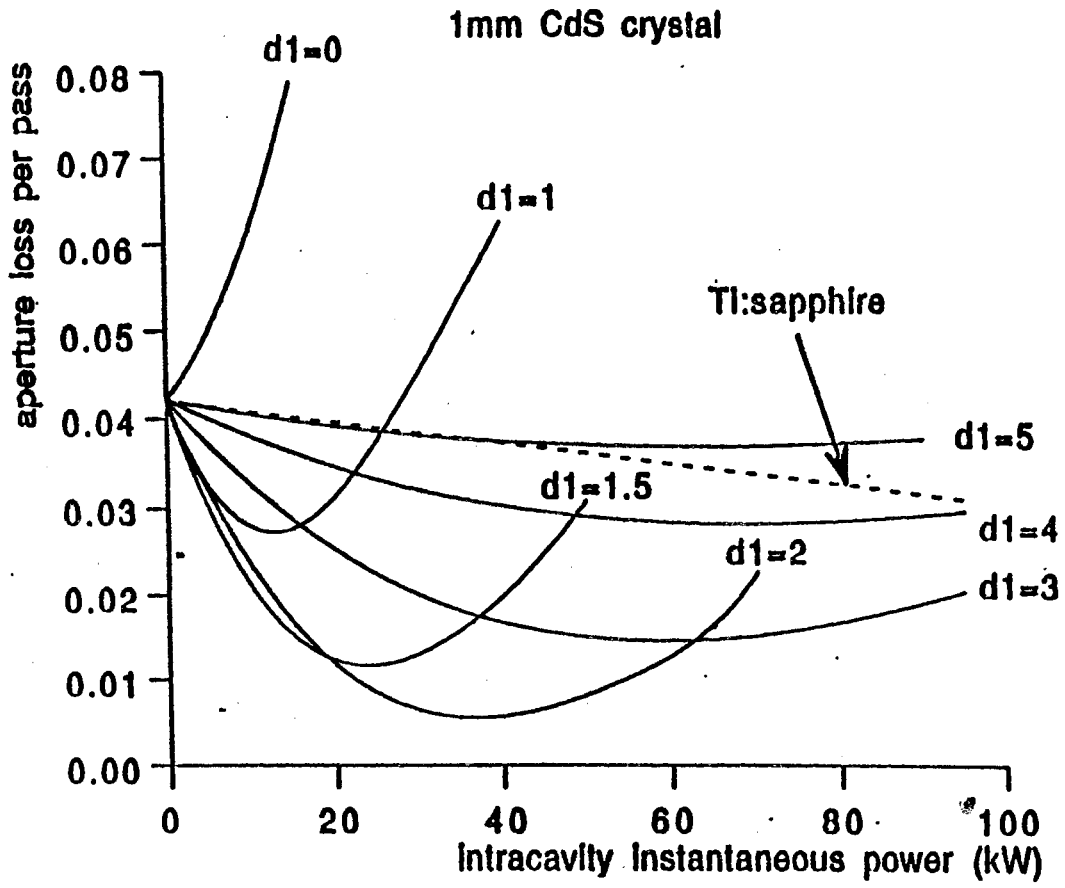

Figure 14. Aperture loss per round trip vs. intracavity power for various crystal positions using thin (1 mm) crystal.

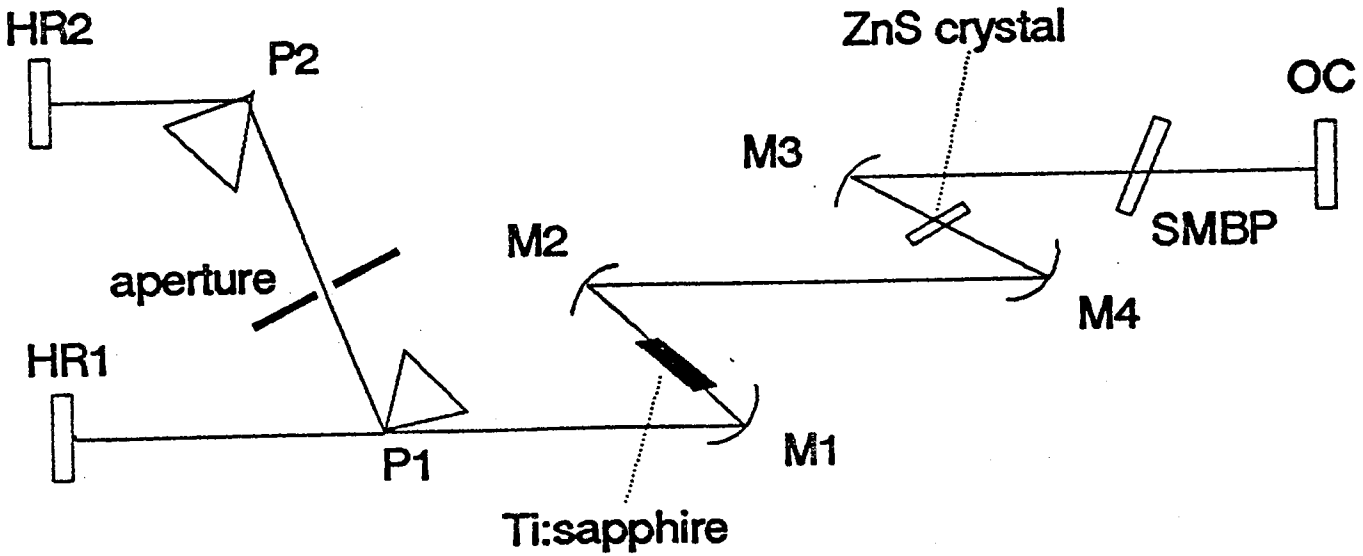

Figure 15. Schematic of experimental linear cavity KLM Ti:sapphire laser with additional self-focusing element in cavity.

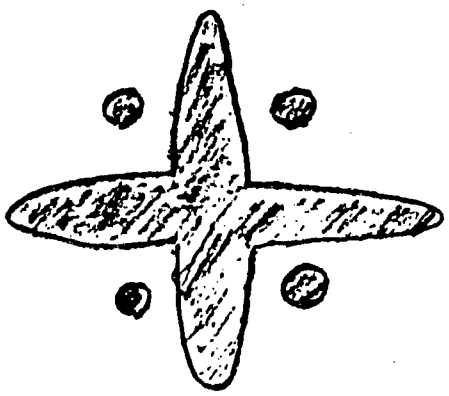

Figure 16. Sketch of beam pattern from laser shown in Figure 15 when system was operating in cw mode, but very close to self-modelocked.

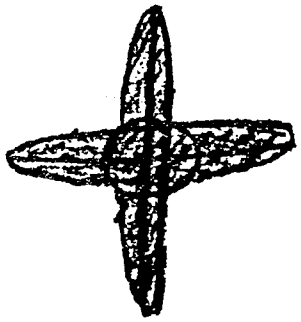

Figure 17. Sketch of beam pattern from self-modelocked KLM laser shown in Figure 15.

VITA

Gary W. Pearson

Candidate for the Degree of

Doctor of Philosophy

Thesis: USE OF ZnS AS A SELF-FOCUSING ELEMENT IN A SELF-STARTING KERR LENS MODELOCKED Ti:SAPPHIRE LASER

Major Field: Electrical Engineering

Biographical:

Personal Data: Born 1955, S. Natick, Mass. Married, one son.

Education: Received Bachelor of Arts in Sociology from Pennsylvania State University, State College, Pennsylvania, in 1976; received Bachelor of Science in Electrical and Computer Engineering from Oklahoma State University, Stillwater, Oklahoma, in 1984; received Master of Science in Electrical Engineering from Rutgers, the State University, New Brunswick, New Jersey, in 1987; completed requirements for Doctor of Philosophy degree at Oklahoma State University in May, 1993.

Professional Experience: Member of Technical Staff, Bell Communications Research, Red Bank, New Jersey, from January, 1985 till January, 1989. Graduate Research Assistant, Electrical and Computer Engineering Dept. and Center for Laser Research, Oklahoma State University, January, 1989 till present.